

	<b>Doc:</b>	Coastcolour-HighRes-ATBD-1.0.doc			
	<b>Date:</b>	25.04.2014			
	<b>Issue:</b>	1	<b>Revision:</b>	0	<b>Page</b>



## **DUE Coastcolour**

### **Algorithm Theoretical Basis Document (SPOT)**

#### **Deliverable DEL-35**

Version 1.0

25. April 2014



<b>Doc:</b>	Coastcolour-HighRes-ATBD-1.0.doc		
<b>Date:</b>	25.04.2014		
<b>Issue:</b>	1	<b>Revision:</b>	0
			<b>Page 2</b>

	<b>Doc:</b>	Coastcolour-HighRes-ATBD-1.0.doc		
	<b>Date:</b>	25.04.2014		
	<b>Issue:</b>	1	<b>Revision:</b>	0

## The Coastcolour Team



**BROCKMANN  
CONSULT**

With



## And the Consultant Team

- Prof. Yu-Hwan Ahn (KORI,
- Dr. Jim Gower (DFO)
- Dr. Mark Dowell (JRC)
- Dr. Stewart Bernard (CSIR)
- Dr. Zhongping Lee (U. Mississippi)
- Dr. Bryan Franz (NASA)
- Dr. Thomas Schroeder and Dr. Arnold Dekker (CSIRO)



<b>Doc:</b>	Coastcolour-HighRes-ATBD-1.0.doc		
<b>Date:</b>	25.04.2014		
<b>Issue:</b>	1	<b>Revision:</b>	0
			<b>Page 4</b>

	<b>Doc:</b> Coastcolour-HighRes-ATBD-1.0.doc			
	<b>Date:</b> 25.04.2014			
	<b>Issue:</b> 1	<b>Revision:</b> 0	<b>Page</b> 5	

## Revision History

Version	Date	Change	Author
1.0	25.04.2014	Initial version	A. Ruescas, BC



<b>Doc:</b>	Coastcolour-HighRes-ATBD-1.0.doc		
<b>Date:</b>	25.04.2014		
<b>Issue:</b>	1	<b>Revision:</b>	0
			<b>Page 6</b>

	<b>Doc:</b>	Coastcolour-HighRes-ATBD-1.0.doc		
	<b>Date:</b>	25.04.2014		
	<b>Issue:</b>	1	<b>Revision:</b>	0

## Contents

1	SCOPE OF THIS DOCUMENT .....	8
2	INTRODUCTION .....	8
3	LITERATURE REVIEW .....	9
4	STUDY SITES .....	15
4.1	Chesapeake Bay.....	15
4.2	Korea .....	16
5	ALGORITHMS' OVERVIEW.....	17
5.1	Background .....	18
5.2	Landsat 5.....	19
5.2.1	Background.....	19
5.2.2	Methods.....	20
5.2.3	Application examples .....	21
5.3	SPOT 4 Take 5.....	26
5.3.1	Background and data assessment .....	26
5.3.2	Methods.....	28
5.3.2.1.	Ratios (Kd490 and TSM comparisons).....	28
5.3.2.2.	The Nechad approach.....	31
5.3.3	Application examples .....	32
5.3.3.1.	MODIS Kd490 test for available pairs .....	32
5.3.3.2.	MODIS TSM (250 m) and SPOT ratio comparison.....	34
5.3.3.3.	Comparison of TSM derived from the Nechad approach on MODIS and SPOT for Chesapeake Bay.....	36
5.4	Rapid Eye .....	44
5.4.1	Background.....	44
5.4.2	Converting RapidEye radiances into reflectances.....	44
5.4.3	Method.....	49
5.4.4	Application examples .....	49
6	ERRORS AND LIMITATIONS .....	51
7	REFERENCES .....	52
8	ACRONYMS AND ABBREVIATIONS.....	53

## 1 SCOPE OF THIS DOCUMENT

This document is the algorithm theoretical basis document for the ESA DUE Coastcolour processing for high resolution data. It is the reference, which specifies the algorithms used on high resolution data to obtain water quality parameters, at least retrieving relative measures for investigating spatial patterns and advantages of the high spatial resolution for questions of coastal processes.

## 2 INTRODUCTION

The objective of this activity within the CoastColour project is to demonstrate the potential of high resolution imagery for coastal water bodies by using, when possible, the 6-month time series of HR optical data (SPOT-4 at 20m resolution and RapidEye at 5m resolution) collected during the SPOT-4 TAKE 5 campaign. Two coastal sites are studied, where CNES acquired SPOT-4 images when the satellite was put into the Sentinel 2 orbit, and where complementary RapidEye and Landsat data are available. This activity is done on preparation for the Sentinel-2 exploitation for water quality applications, in terms of demonstrating the advantages of the high spatial resolution and to cope with the limitations in available spectral bands as well as the reduced radiometric sensitivity. Sentinel 2 band distribution along the electromagnetic spectrum is shown in Fehler! Verweisquelle konnte nicht gefunden werden..

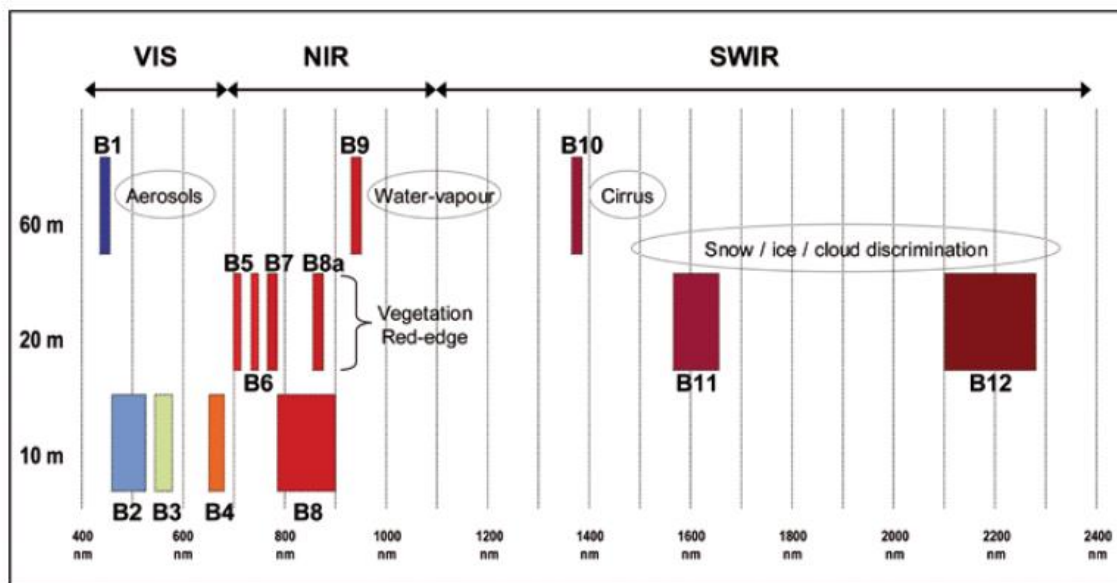


Figure 1 Sentinel 2 spectral bands vs. spatial resolution (from ESA Special Publication 1322/2)

The easiest case for coastal ocean colour remote sensing are sediment dominated turbid case 2 waters without much chlorophyll or CDOM content, where the signal in the longer wavelengths is dominated by backscatter from the water. There is a simple, almost linear relationship between backscatter (or scattering) and marine reflectance even in single bands (Doxaran et al., 2002; Kallio et al., 2008). The backscatter can then be converted into parameters such as TSM or turbidity.

The two study areas are:

- Chesapeake Bay (US east coast), which is the primary test and validation site of NASA and NOAA.

- Korean waters: which are partly highly turbid and thus favouring the scattering approach.

A literature review was made (**Fehler! Verweisquelle konnte nicht gefunden werden.**) in order to understand and apply the already operational methods used to extract water quality parameters from high resolution sensors like the ones on board of the Landsat satellites (TM, ETM, ETM+) , SPOT (XS) or Rapid Eye.

### 3 LITERATURE REVIEW

In most of the papers reviewed Landsat is used to derive total suspended matter (TSM) or turbidity values in estuaries or high turbid waters. To a lesser extent, chlorophyll concentration or absorption of yellow substance is also calculated.

Dekker et al. (2001) used data from Landsat-TM5 and SPOT-HRV to derive TSM maps in the southern Frisian lakes in the Netherlands. The algorithms were based on analytical optical modelling using the in situ inherent optical properties. The spectral bands 2 and 3 of TM and XS1 and XS2 from SPOT show an almost equivalent behaviour with increasing TSM. Band TM4 seems to be the most suited for inversion because of its linearly increasing function; however, they did not use it because of the less SNR in this domain and problems with the adjacency effect.

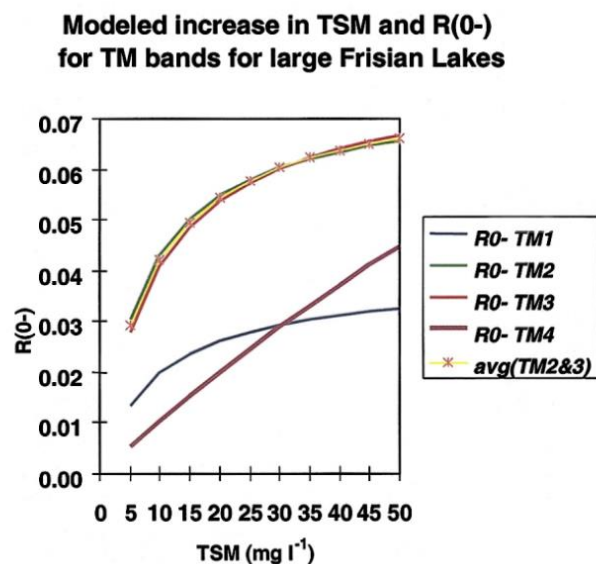


Figure 2 The analytical relationship between R(0-) in Landsat -TM bands 1,2,3 and 4 and TSM for an average set of Frisian large lakes (from Dekker et al., 2001)

Doxaran et al. (2002a and 2002b) focused their attention in the Gironde estuary and used SPOT-HRV bands and SPM in situ measurement concentrations to derive TSM from the satellite images. The remote sensing reflectance increase together with the increase of SPM is observed, and based on this assumption SPOT XS1, XS2 and XS3 are used to determined SPM concentration using ratios in an empirical approach.

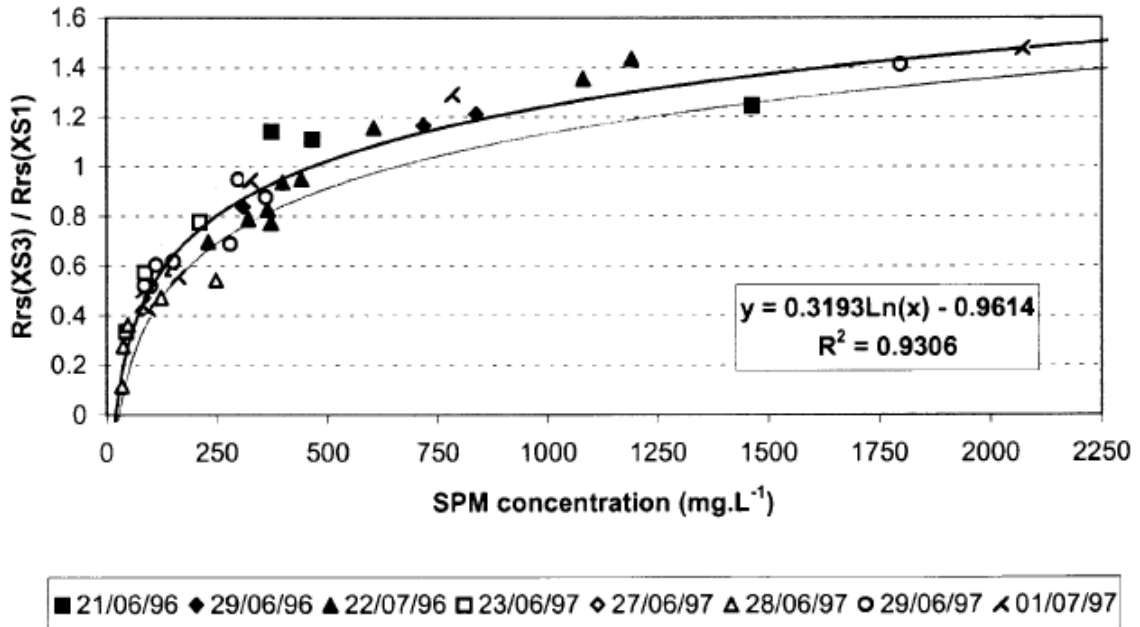


Figure 3  $Rrs(XS3)/Rrs(XS1)$  band ratio vs. SPM concentration, The function is log (second rate) with a correlation factor of 0.935 (from Doxaran et al., 2002a)

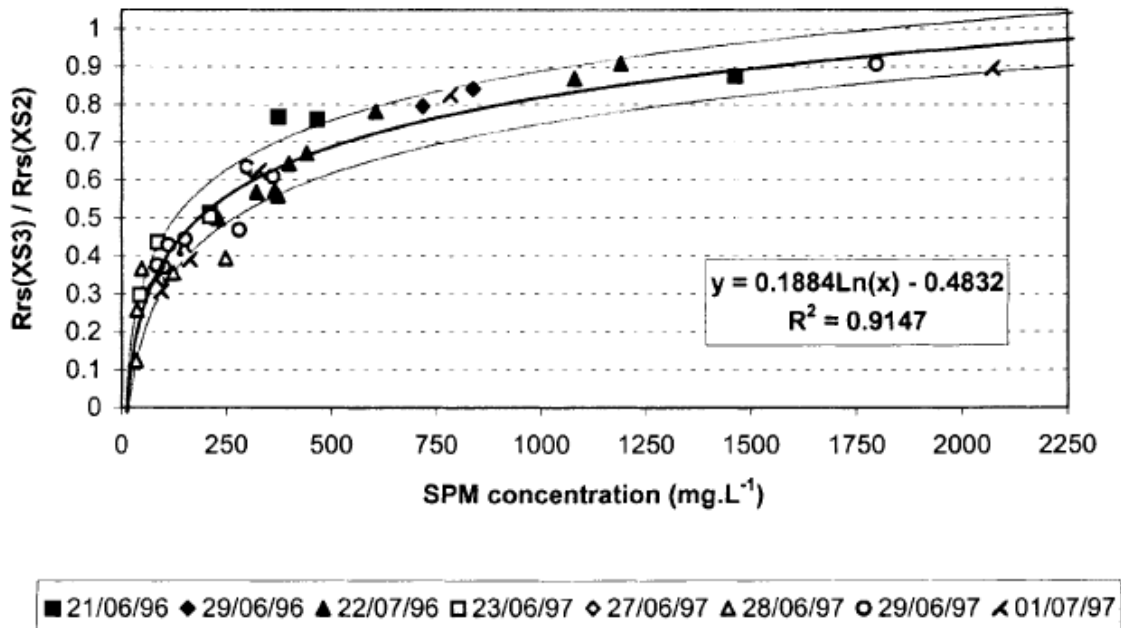
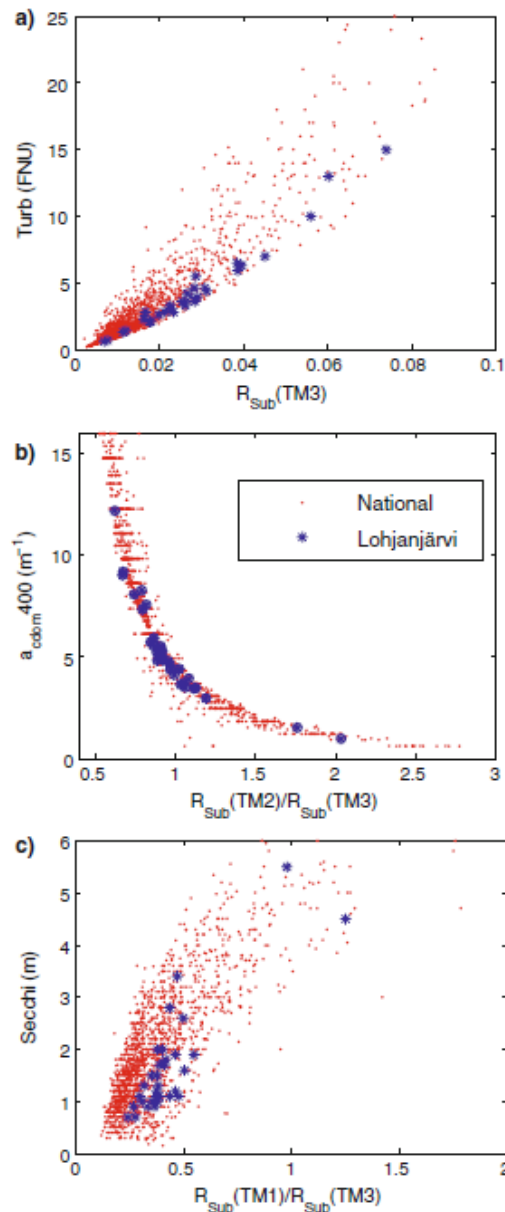


Figure 4  $Rrs(XS3)/Rrs(XS2)$  band ratio vs. SPM concentration, The function is log (second rate) with a correlation factor of 0.917 (from Doxaran et al., 2002a)

Kallio et al. (2008) investigated the use of Landsat ETM+ images in monitoring of turbidity, coloured dissolved organic matter absorption ( $a_{CDOM}$ ), and Secchi disk depth ( $Z_{SD}$ ) in lakes of two river basins located in southern Finland. They also used an empirical approach to derive water quality algorithms from Landsat scenes. Several linear and exponential relationships are tested between the in

situ measurements and the ETM+ data with form  $y=(a*x)+ b$  and  $y=a*e^{b*x}$ , where  $y$  is the turbidity,  $a_{CDOM}$ , or  $Z_{SD}$ ,  $x$  is the reflectance of one channel or the reflectance ratio of two channels, and  $a$  and  $b$  are empirical coefficients. The selection of  $x$  is based on previous studies: TM3 for turbidity, TM2/TM3 for  $a_{CDOM}$ , and TM1/TM3 for  $Z_{SD}$ .



**Figure 5** Relations between simulated subsurface reflectance and reflectance ratios and measured turbidity,  $a_{cdom}(400)$  and  $Z_{sd}$  in lake Lohjanjärvi in 2002 (from Kallio et al. 2008)

Ma and Dai (2005) calculated chlorophyll (CHL) and total suspended matter (TSM) combining Landsat ETM bands, and using again an empirical approach with in situ measurements in the Taihu lake. For the estimation of the CHL concentrations they use a regression analysis between CHL in situ and ratio of bands ETM4/ETM3 and TM4 and ETM2. The stronger correlation was between the ratio with band in 706 nm (ETM4) and band in 682 nm (ETM1) and the chlorophyll concentrations in situ; followed by the log base e curve-fitting between ETM3 and the CHL in situ. The TSM concentration has

a strong correlation with ETM4. They made several tests with different macropixel sizes of the Landsat pixels and try the different algorithms to study how the spatial resolution affected the accuracy of the results (see Figure).

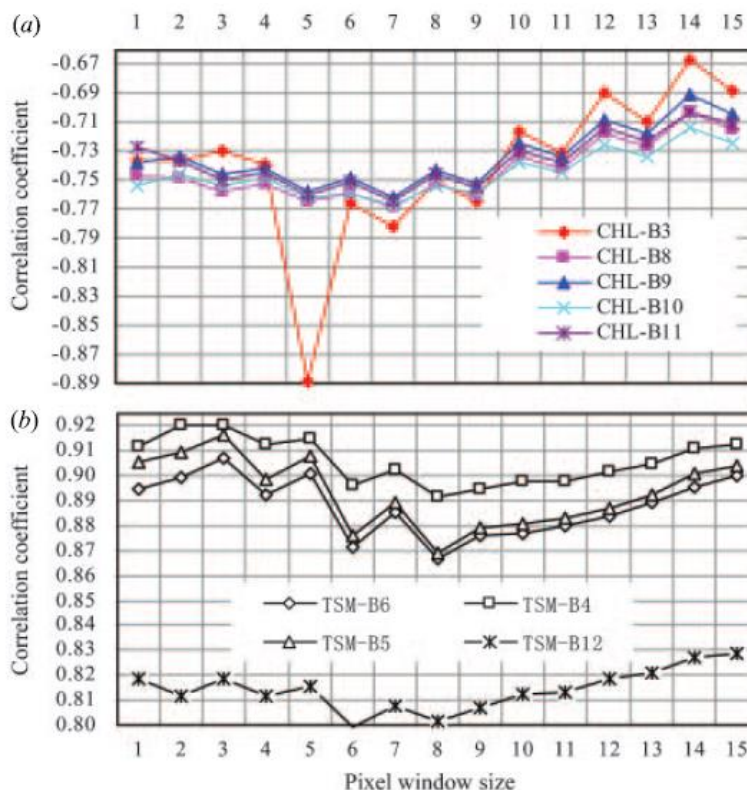


Figure 6 Correlation between CHL (a) and TSM (b) concentrations and different pixel window sizes (from Ma and Dai, 2005)

Nechad et al. (2010) did not apply the TSM concentration derivation to any high resolution sensor, but they developed a basic TSM algorithm for turbid waters suitable for any ocean colour sensor. They performed a hyperspectral calibration using seaborne TSM and reflectance spectra collected in the southern North Sea. Applying a non-linear regression analysis to the calibration dataset gave relative errors in TSM estimation less than 30% in the spectral range 670-750nm. This work is used as a reference to develop specific SPOT TSM algorithms using a single spectral band and the empirically derived hyperspectral coefficients (see Table 1 and Table 4 in referenced paper).

This approach developed by Nechad has been subsequently used in many other projects, like the one by Vanhellemont and Ruddick (2014) in the Thames estuary. They applied the single band algorithm to Landsat 8-OLI band 630-680 nm (OLI4) and 845-885 nm (OLI5), and compared the results with MODIS/Aqua derived TSM applying the same equation to band 645 nm. The results show a TSM pattern in the OLI and MODIS products very coherent, and absolute retrievals in good agreement, especially considering the temporal dynamics of the region and the large differences in viewing conditions and sensor design. Vanhellemont and Ruddick concluded that the high spatial resolution resolves small scale turbidity features, and the high patchiness in the suspended sediments in coastal waters can be studied.

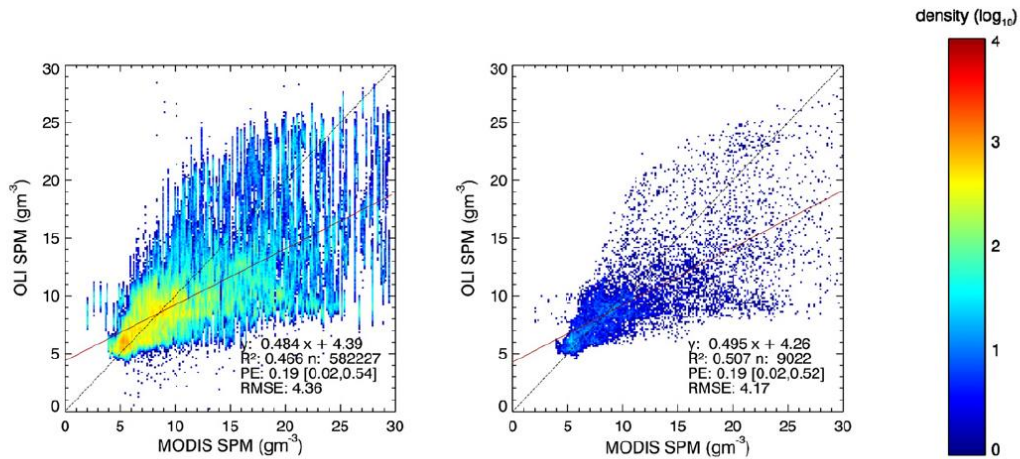


Figure 7 Comparison of OLI against MODIS data -OLI resolution left; MODIS resolution right-. The colours denote pixel densities in log scale. The dashed line is the 1:1 line, the solid red line is the ordinary least squares regression line (from Vanhellemont and Ruddick, 2014)

The last paper reviewed is Wang et al. (2009). The study area is the Yangtze River in China and the sensor used is Landsat ETM+ together with in situ SSC (suspended sediment concentrations). Again, the method is an empirical approach based on the possible correlations of the reflectance ETM+ bands and the SSC observed. For this area ETM3 reflectance shows an increase with increasing SSC, saturating with SSC values >600 mg/l. The saturation threshold is higher in ETM4 and this is the band finally used for the TSM algorithm derivation (in natural logarithmic values).

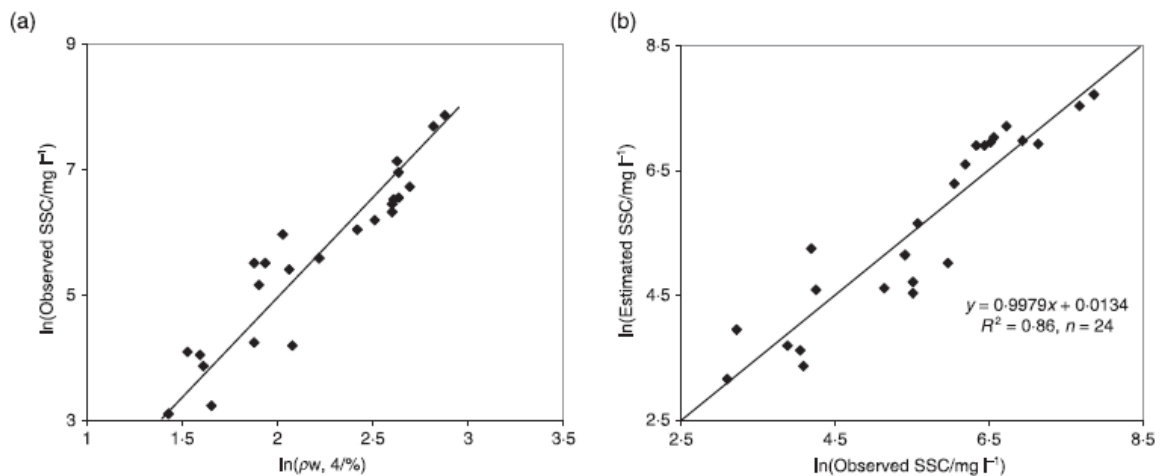


Figure 8 Results of regression between SSC and water reflectance at band 4 within the range 22-2610 mg/l in the Upper and Middle Yangtze River. (a) Calibration of the algorithm (b) validation results (from Wang et al. 2009)

**Table 1 Literature review of methods for estimation of water quality parameters using high resolution sensors**

	SPOT	Landsat	AC method	In water algo	Area of study	In situ data for calibration/concentration range	Observations
Dekker et al. (2001)	XS1(510-590nm), X2 (610-680nm), XS3 (790-890nm)	TM1(450-520) TM2(520-600) TM3(630-690) TM4(760-900)	MODTRAN 3	$0.7581\exp[61.683(RrsTM2/RrsTM3)]$ or $0.7581\exp[61.683(RrsXS2/RrsXS3)]$	Southern Frisian lakes	Chlorophyll concentration up to $300 \mu\text{g L}^{-1}$ SD as low as 20 cm	TM4 not used, it could be affected by adjacency effect; algos less sensitive for TSM > $40\text{mg l}^{-1}$ due to saturation
Doxaran et al. (2002a)	XS1(510-590nm), X2 (610-680nm), XS3 (790-890nm)		6s	Empirical: $Rrs(XS3)/Rrs(XS1) = 0.3193\ln(\text{SPM}) - 0.9617$ Empirical: $Rrs(XS3)/Rrs(XS2) = 0.1884\ln(\text{SPM}) - 0.4832$	Gironde stuary	SPM/35-2072 $\text{mg l}^{-1}$	Correlation coefficients > 0.9 Error < 40%
Doxaran et al. (2002b)	XS1(500-590nm), X2 (610-680nm), XS3 (790-890nm)	L7 ETM3 (525-600nm) ETM5 (845-885nm)	Not mentioned	$Rrs(850)/Rrs(550)$	Gironde stuary	TSM/0.013-0.985 $\text{g l}^{-1}$	Uncertainty of $\pm 7\%$
Kallio et al. (2008)		ETM +	Not mentioned SMAC: the AC produced a slight improvement in the overall estimation accuracy of aCDOM and Zsd. In the case of turbidity, the estimation accuracy was about the same (turbidity from TOA calculated from a ratio)	$RrsTM3(630-690\text{nm})$ for turbidity = $385TM3-1624$ $RrsTM2(530-610\text{nm})/RrsTM3(630-690\text{nm})$ for aCDOM = $23.33\exp[-0.97(TM2/TM3)]$ $RrsTM1(450-520\text{nm})/RrsTM3(630-690\text{nm})$ for Zsd = $1.806(TM1/TM3) - 0.8903$ Turbidity with TOA = $2389\exp[-2.72(TM1/TM3)]$	Karjaanjoki and Siuntionjoki Lakes	aCDOM(440)/1.0-12.2 $\text{m}^{-1}$ Zsd/0.6-25 FNU turbidity/2.4-80 $\mu\text{g L}^{-1}$	Errors: CDOM 17.4%; Zsd 21.1%; turbidity 23% (coefficient of determination and rmse)
Ma and Dai (2005)		ETM+	Darkest pixel using B7	$TSM2 = 1799.554 * (ETM4/ETM1) - 209.074$ $TSM1 = 0.221 * (ETM4)^2 + 60.293$ $CHL1 = -0.054 * ETM3 + 6.676$ $CHL2 = -167.55 * \ln(ETM3/ETM1) - 48.137$	Taihu Lake	22 water samples +11 water samples from another observatory; in situ spectrum measurements	
Nechad et al. (2010)		Adapted to MERIS, MODIS and SeaWiFS, but coefficients calculated every 2.5 nm between 520-885nm	in situ reflectances	TSM concentration or $S = (A^0 \rho_w / (1 - \rho_w C^0)) + B^0$	North Sea	441 water-leaving reflectances; TSM measurements	Algorithm development using hyperspectral in situ data. Single band algorithm based on reflectance model calibrated using in situ reflectance and TSM measurements. The algorithm is not well suited to use wavelengths less than 600 nm (Cp set to $14.49 \cdot 10^{-2}$ )
Vanhellemont and Ruddick (2014)		OLI 4 (630-680nm) 5 (845-885 nm)	Average similarity spectrum method (Ruddick et al., 2006)	TSM concentration or $S = (A^0 \rho_w / (1 - \rho_w C^0))$	Thames estuary	SPM/0.5-100 $\text{g m}^{-3}$	Comparison of TSM results with MODIS (250m). Spatial resolution impact: increased vertical striping in scatterplots. RMSE increases from 0.425 to 1.1 from 150 to 900 m resizing of the Landsat data. Other factors leading to errors: different viewing conditions and sensor design; time difference between scenes
Wang et al. (2009)		ETM +	Use of ETM+7 (SWIR, 2080-2350nm), after Rayleig correction, to subtract glint and aerosol path reflectance	$\ln(\text{SSC}) = 3.18236\ln(RrsTM4) - 1.4006$ ( $RrsTM3/RrsTM5$ ) and ( $RrsTM4/RrsTM1$ ) also recommended in case with low chlorophyll concentrations	Yangtze River	SSC/22-2610 $\text{mg l}^{-1}$	Coefficient of determination 0.88

## 4 STUDY SITES

### 4.1 Chesapeake Bay

Chesapeake Bay is the Site 6 of the CoastColour project (Figure 9). This region shows high values of spectral downwelling attenuation coefficient ( $k_d$ ) at all measured wavelengths. Using the CoastColour database as reference, the maximum value is  $1.7625 \text{ m}^{-1}$  at 411 nm, the minimum is  $0.0411 \text{ m}^{-1}$  at 489 nm. The total chlorophyll a values, 12 measurements, fluctuate between  $0.3 \text{ mg/m}^3$  and  $22.54 \text{ mg/m}^3$ . Maximum depth for 37% light level of PAR is 9.2 m, 22.8 m for 10 % and 42.7 m for 1 % light level of PAR. The CoastColour in-situ database contains various measurements of Lw at wavelengths between 411 nm and 683 nm. Between 80 and 171 measurements of Lw are contemporary of Chl\_a,  $k_d$  ( $k_d411$ ,  $k_d433$ ,  $k_d489$ ,  $k_d510$ ,  $k_d530$  and  $k_d555$ ),  $z_{37}$ ,  $z_{01}$  and  $z_{10}$  in each MERIS band.

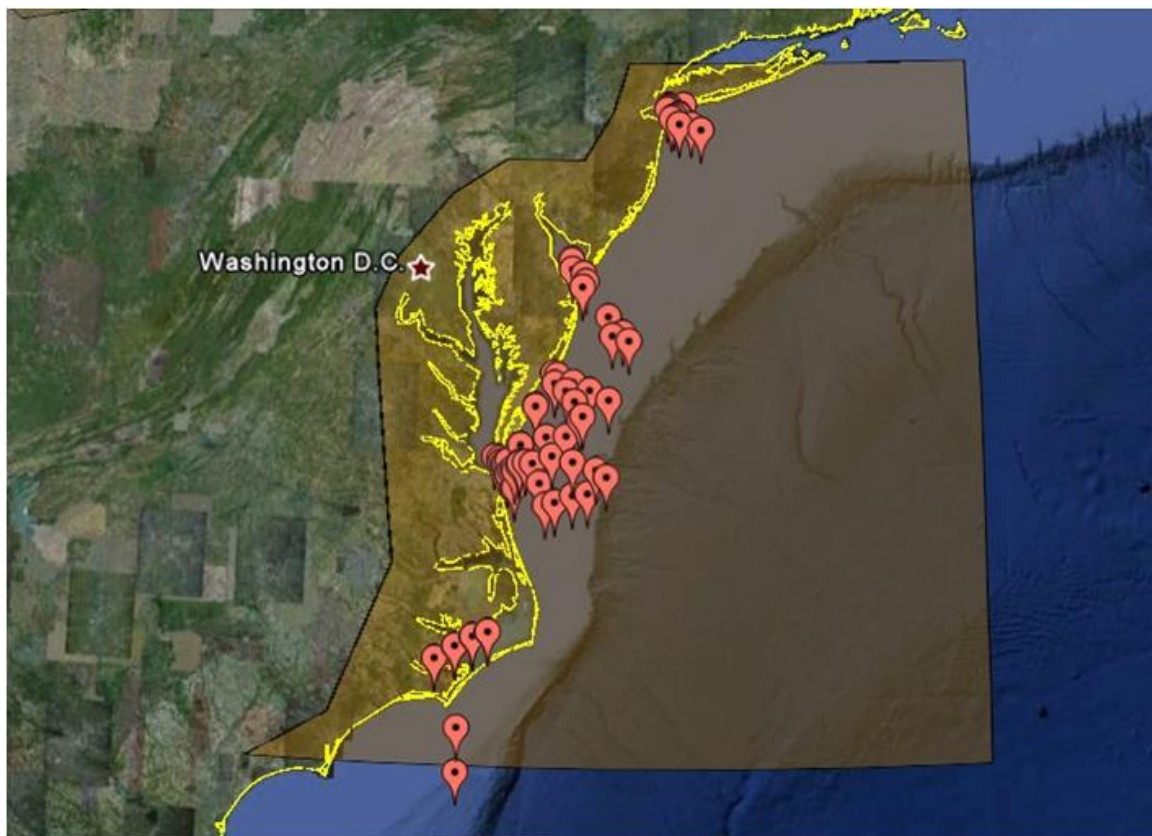


**Figure 9** Location of the matchups of in situ and MERIS products in the Chesapeake area

The area covered by the SPOT 4 Take 5 mission is a small rectangle inside the bay and outside the region of the CoastColour matchups (Figure 10).

The Mermaid matchup database also contains a few in situ data on the Chesapeake area, but none of the 6 in situ station falls inside the SPOT 4 Take 5 region.

The CoastColour database as well as MERMAID are then of limited use for this study, which represents not a major problem because the SPOT satellite data are from 2013, while the ENVISAT satellite stop transmission of MERIS data in April 2012.

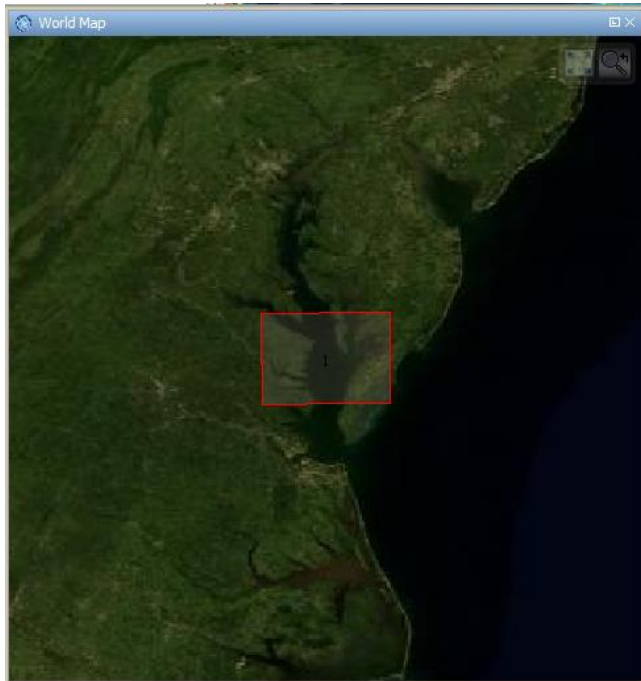


Figure 10 Area covered by the SPOT 4 Take 5 inside the Chesapeake Bay

## 4.2 Korea

The Korea study area is part of the Site 11 of the CoastColour project. Site 11 comprehends China, Korea and Japan waters. The SPOT 4 TAKE 5 data were taken along the northwest coast of Korea (Figure 11).

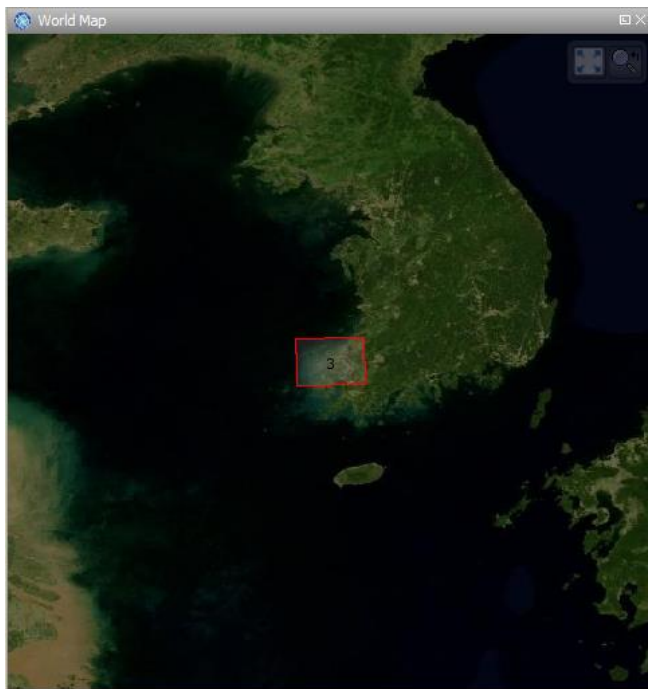


Figure 11 Area covered by the SPOT 4 Take 5 in South Korea

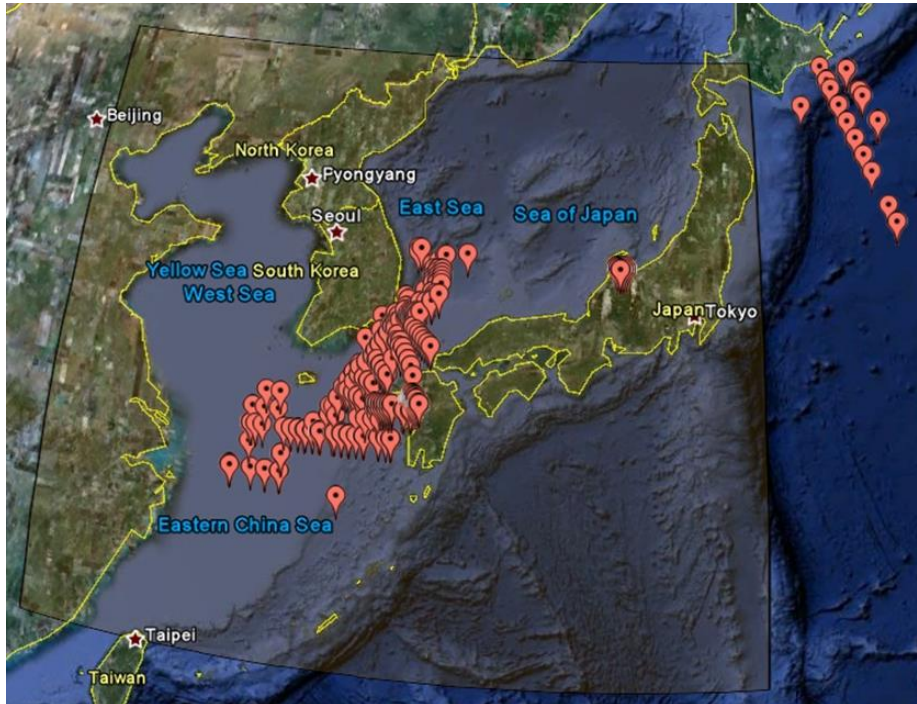


Figure 12 Location of the matchups of in situ and MERIS products in the Site 11

The CoastColour in-situ database includes data for test site 11 for regions with 48 to 2198 m water depth mostly in the East Sea and the East China Sea (Figure 12). Water temperature comprises the range between 1.9 °C and 23.1 °C. Both minimum and maximum of the spectral downwelling attenuation coefficient ( $k_d$ ) were measured at 490 nm ( $0.009 \text{ m}^{-1}$  and  $2.471 \text{ m}^{-1}$ ). Salinity varies between 21.15 and 34.75 psu, while the density is 25.32-26.91 sigma. The concentrations of TSM are generally below 5 mg/l but reach values of up to 22 mg/l in some cases. The same can be said about chlorophyll and POC. Chlorophyll shows higher concentrations than 5 mg/m<sup>3</sup> in exceptional cases, with 71.63 mg/m<sup>3</sup> registered as a maximum value. Particulate organic carbon exceeds the most frequent concentration of up to 5 mg/m<sup>3</sup> in some cases and then reaches very high values of 90.9 mg/l. CDOM varies between 0. and 0.517.

## 5 ALGORITHMS' OVERVIEW

One important point to highlight is the non-existent in situ measurements (reflectance or IOPs) for the Chesapeake and Korea regions coincident in space and time with the high resolution data acquired during SPOT4 TAKE 5 experiment. The lack of in situ references constrained the analysis and development of algorithms, because the empirical method is the predominant approach in most of the literature review. This means that results are not quantitatively comparable, and the analysis is focused on the trend analysis and spatial pattern recognition in the different scenes compare with standard MERIS or MODIS turbidity or TSM products. In Figure 13 there is a flow chart with the different datasets and methods followed: on the left Landsat data and MERIS data WQ products were analysed using linear and non-linear regression analysis. On the right the same regression analysis was made to pairs of data of SPOT 4 take 5 and MODIS WQ products. The methods to derived data from HR sensors like Landsat or SPOT is limited to band ratios or application of coefficients to one band (Nechad et al., 2010).

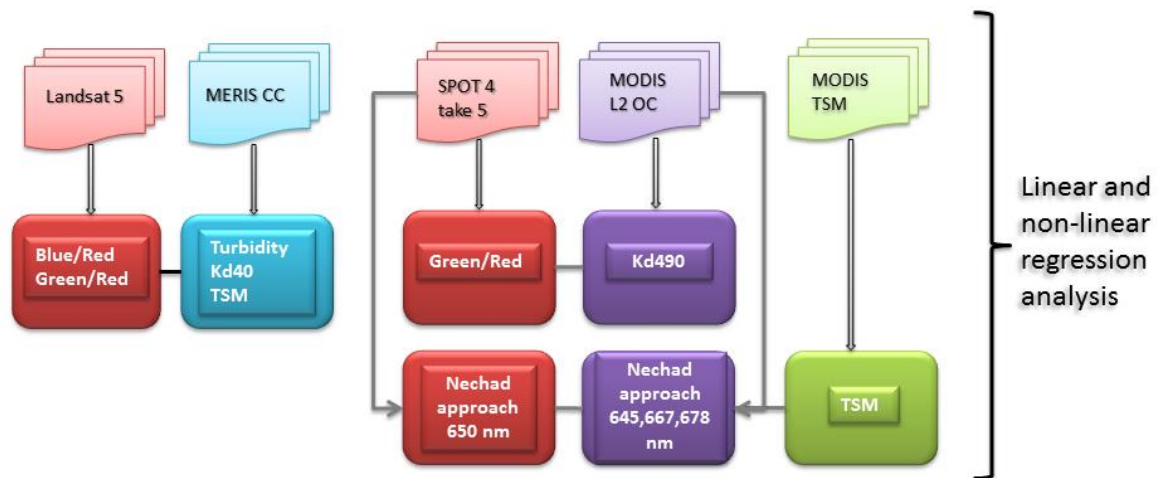


Figure 13 Datasets and methods followed in the development of the algorithm for WQ products from HR data

## 5.1 Background

On January 29 2013, SPOT4's orbit was lowered by 3 kilometres to put it on a 5 day repeat cycle orbit. On this new orbit, the satellite flew over the same places on earth every 5 days. SPOT 4 followed this orbit until June the 19th, 2013. During this period, 45 sites were observed every 5 days, with the same repeat cycle as Sentinel-2. The data have been processed and distributed by the THEIA Land data center and distributed to users in mid July 2013.

In Fehler! Verweisquelle konnte nicht gefunden werden., published algorithms for water quality retrieval were summarised. In order to check the validity of the most promising of these (mainly) ratio algorithms, and to link them to CoastColour products, these should be compared with the corresponding values from MERIS. However, MERIS data were no longer available at the time of SPOT-4 Take 5 experiment. This is the reason why the algorithm study was performed on the analysis on Landsat 5 TM data on the Chesapeake area. Landsat 5 is radiometrically closer to Sentinel 2 than SPOT 4 (Figure 14).



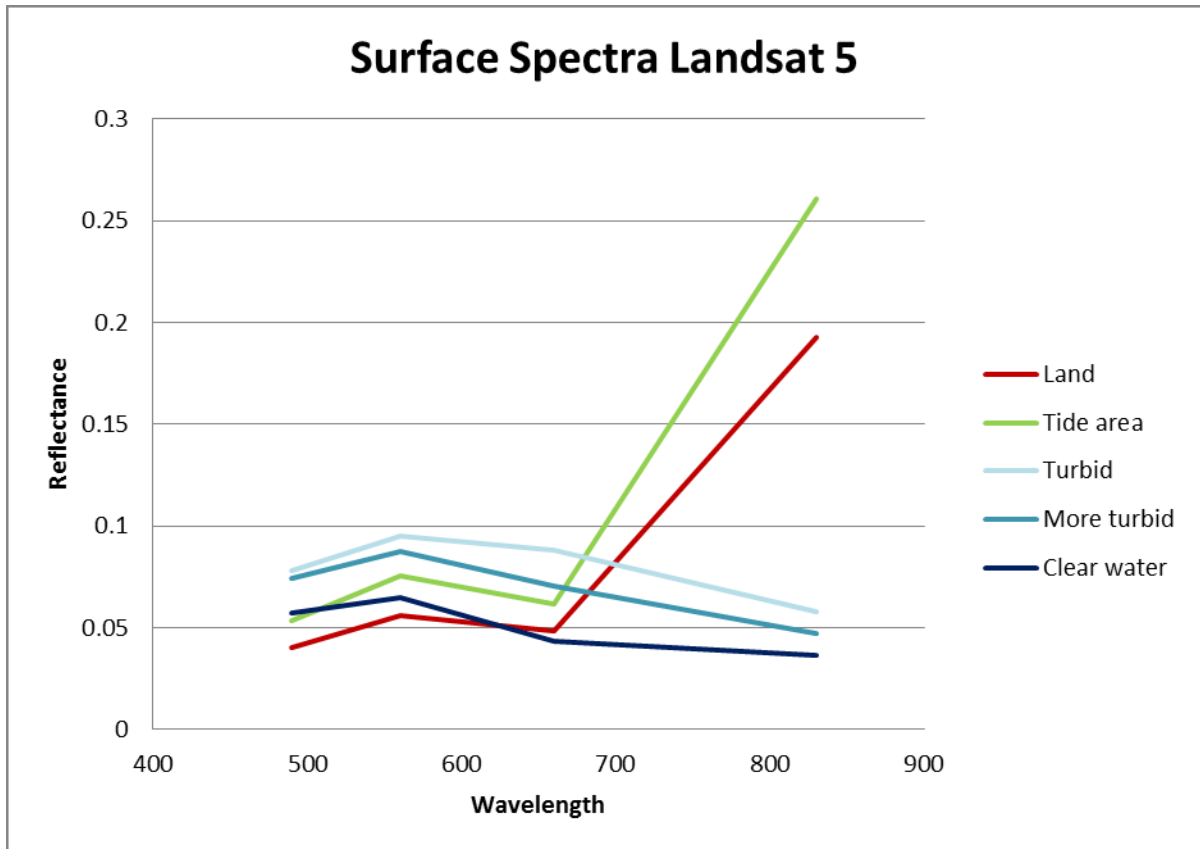


Figure 15 Examples of reflectance behaviour of some surface in the atmospherically corrected Landsat-5 images

#### 5.2.2 Methods

Four different ratios were calculated (see Fehler! Verweisquelle konnte nicht gefunden werden. and Figure 17): the ratio  $TM1 (0.45 - 0.52 \mu m) / TM3 (0.63 - 0.69 \mu m)$  for turbidity from Kallio et al. (2008); the Secchi Depth ratio  $TM2 (0.52 - 0.60 \mu m) / TM3$  of Dekker et al. (2001); the ratios  $TM4 (0.76 - 0.90 \mu m) / TM1$  and  $TM3 / TM1$  from Mai and Dai (2005).



Figure 16 Landsat image RGB composition, pixel aggregated to 300 m and collocated to the corresponding MERIS image

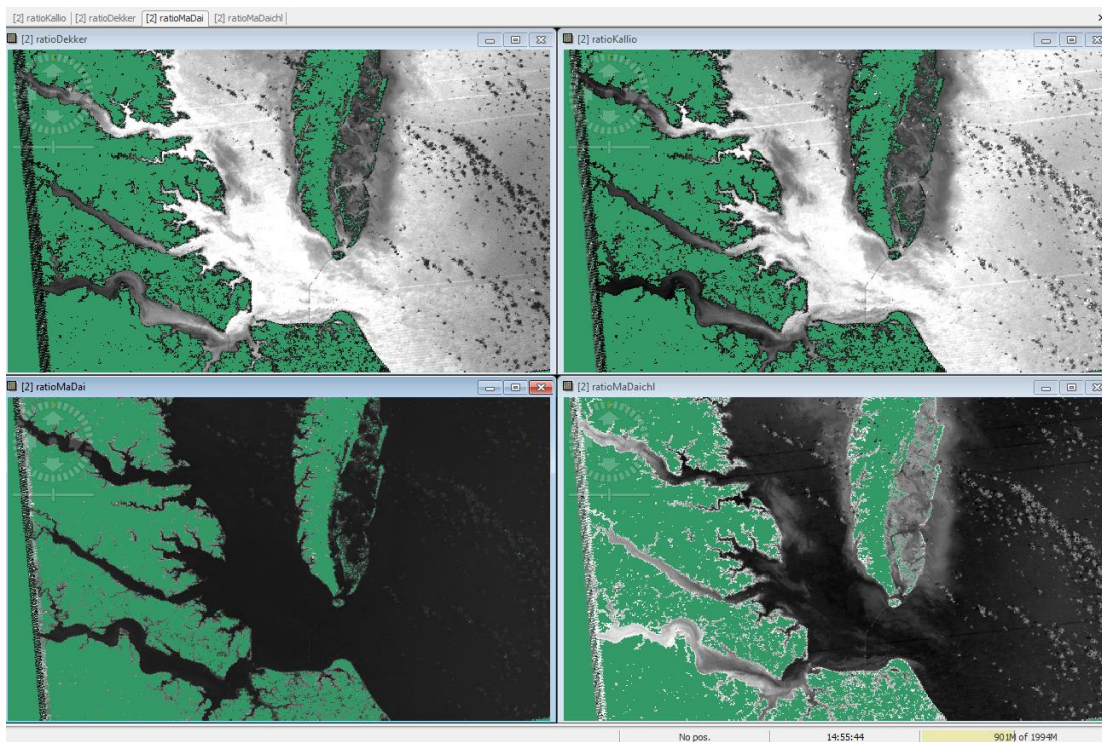


Figure 17 Results of ratios with ETM bands: top left TM2/TM3; top right TM1/TM3; bottom left TM4/TM1; and bottom right TM3/TM1

### 5.2.3 Application examples

The transect running in between the areas called Webbs and Rogue Islands, and penetrating into the open sea, is showed in Figure 18. The values of the four Landsat reflectance ratios as well as the products derived from MERIS using the CoastColour algorithm: Kd490, turbidity and total suspended matter were extracted for all pixels along the transect.

In Figure 19, there are two scatter plots showing the relation between the “Kallio” TM ratio (blue/red) and the “Dekker” TM ratio (green/red) with the MERIS values for turbidity. This relation adjusts very well to an exponential regression type for both cases. This exponential relation was already observed by Kallio et al. (2008). They indicated that this type of regression -in their case using top of atmosphere bands- of the turbidity value measured in situ with the ratio of bands TM1 and TM3, gives the best results in terms of coefficient of determination (0.83) and root mean square error, 22.3% (rsme). The Kd90 and TSM parameter relationship with the blue/red ratio are shown in Figure 20. In both cases the exponential regression line has the best adjustment, as expected, but also all other relationships (linear, polynomial and logarithmic) give very reasonable results.

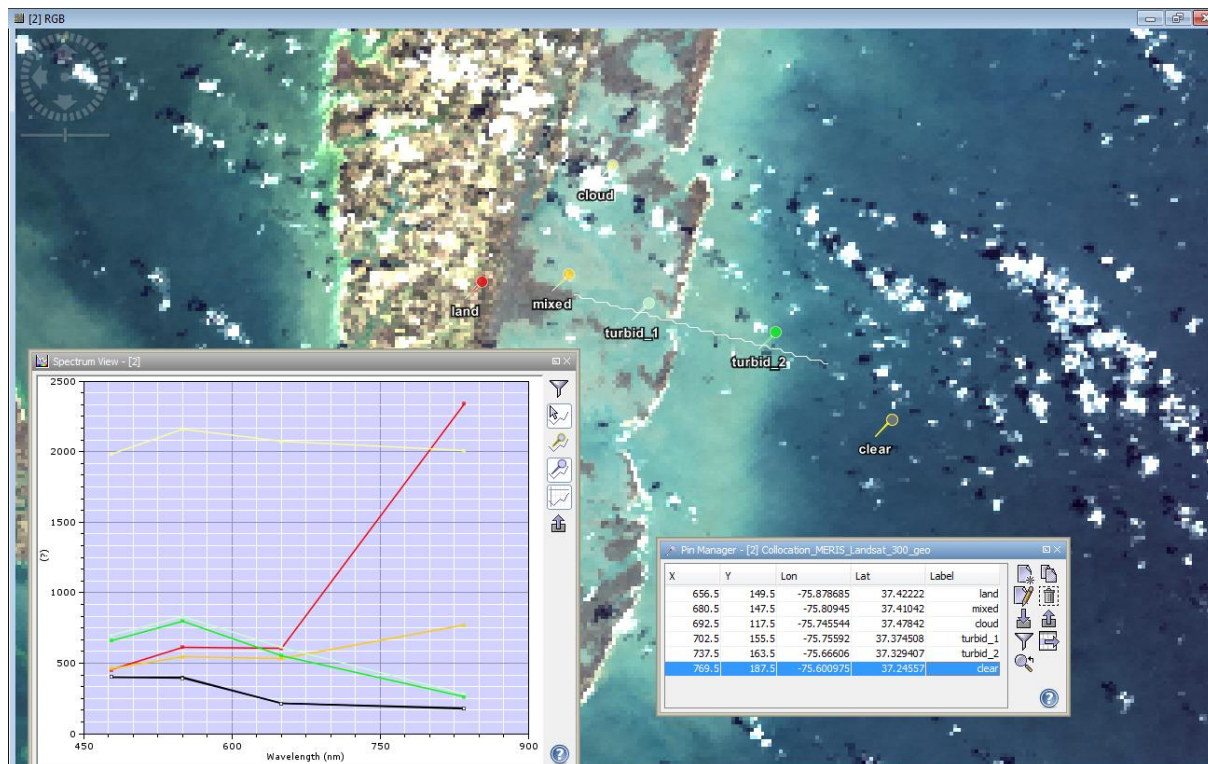


Figure 18 Spectrum view on the reflectance of the different surfaces (land, mixed, cloud, turbid\_1, turbid\_2 and clear). Pin locations are shown on the RGB Landsat image, as well as the transect (in white) drawn for building the scatter plots explain in the text and shown in Figure 17.

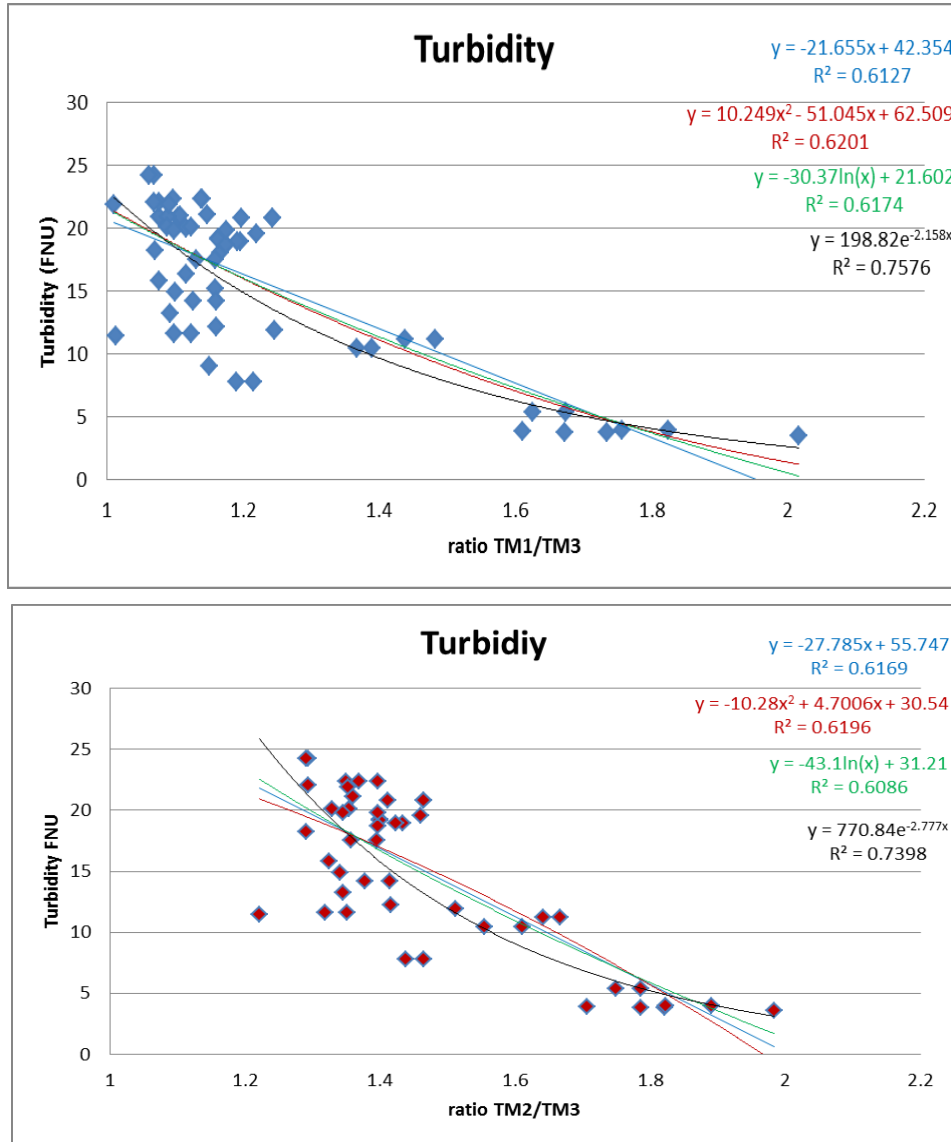


Figure 19 Different regression relations between the TM ratio blue-red and green-red and the MERIS turbidity values

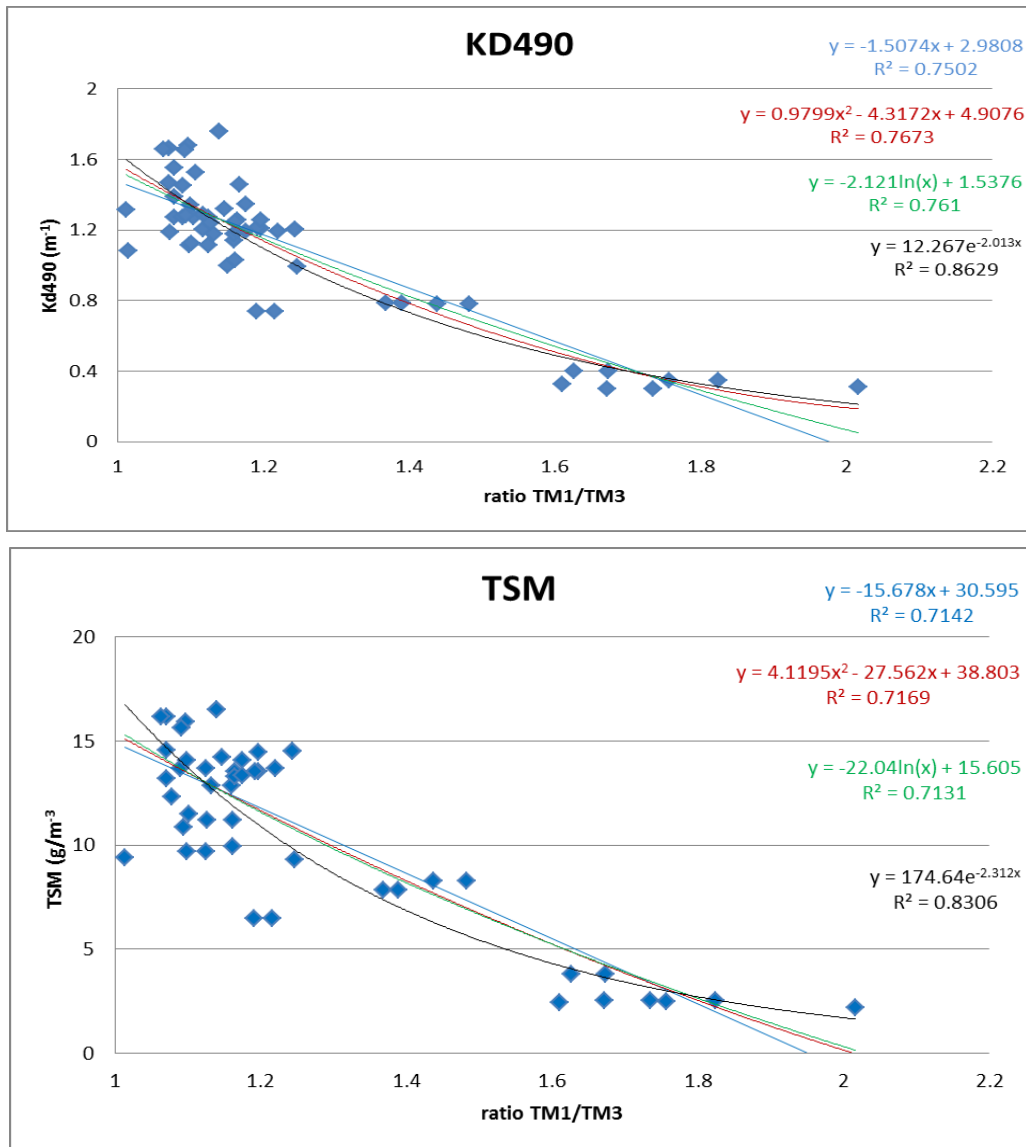


Figure 20 Different regression relations between the TM ratio blue-red and the MERIS Kd490 and TSM values

The three equations to calculate TSM, turbidity and Kd are applied to the different band combinations for one Landsat image and results compared with a MERIS image from a close date.

Figure 21 shows the TSM concentration calculated using  $TSM = 174.36e^{-2.312(TM1/TM3)}$

Equation 1 on the Landsat 5 from 28-02-2008. Below the TSM from MERIS calculated using the CC algorithm. Notice that there is a day of difference in between them.

$$TSM = 174.36e^{-2.312(TM1/TM3)}$$

Equation 1

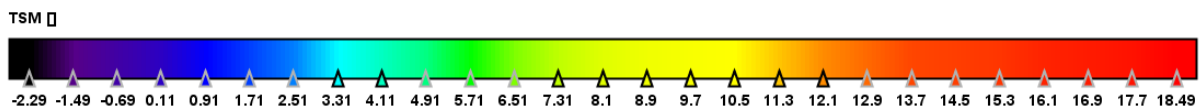
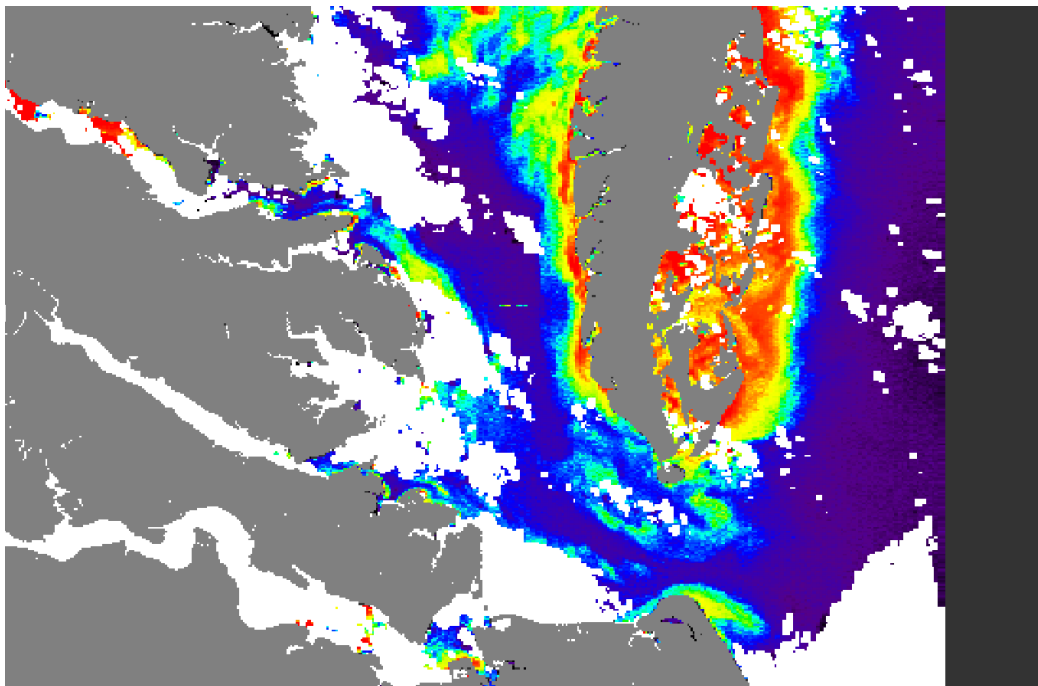
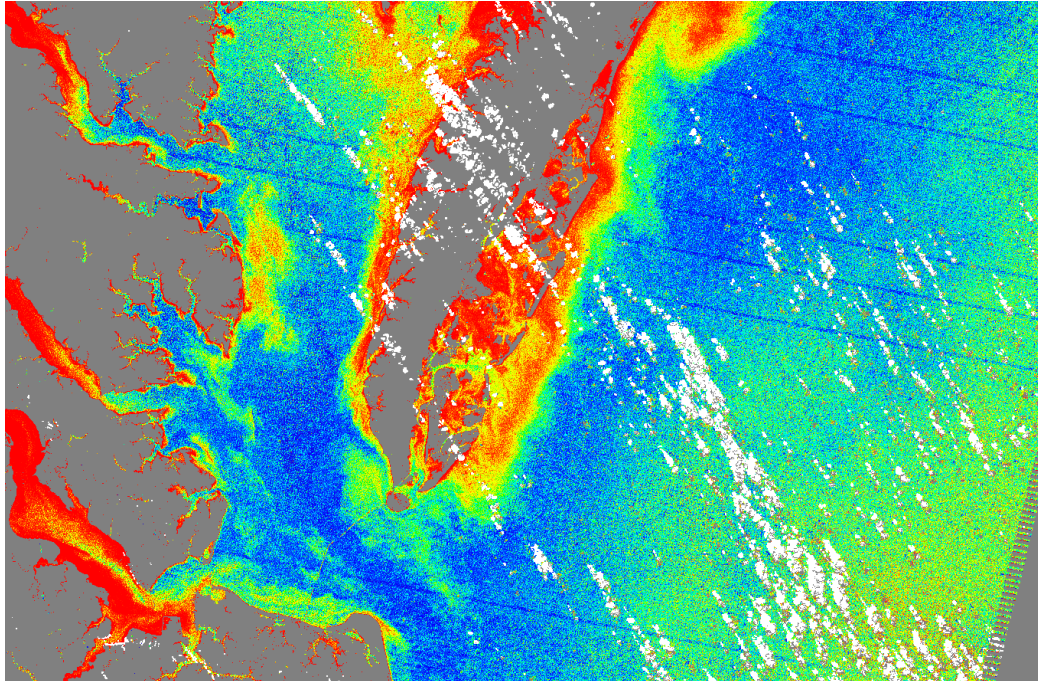


Figure 21 On the top, TSM product derived from Landsat 5 (LT50140342008059GN01) using the exponential expression. In grey the land mask and in white the cloud, cloud shadows and cloud adjacency masks. On the bottom, TSM product derived from the Coast Colour algorithm from MERIS (2008-02-27)

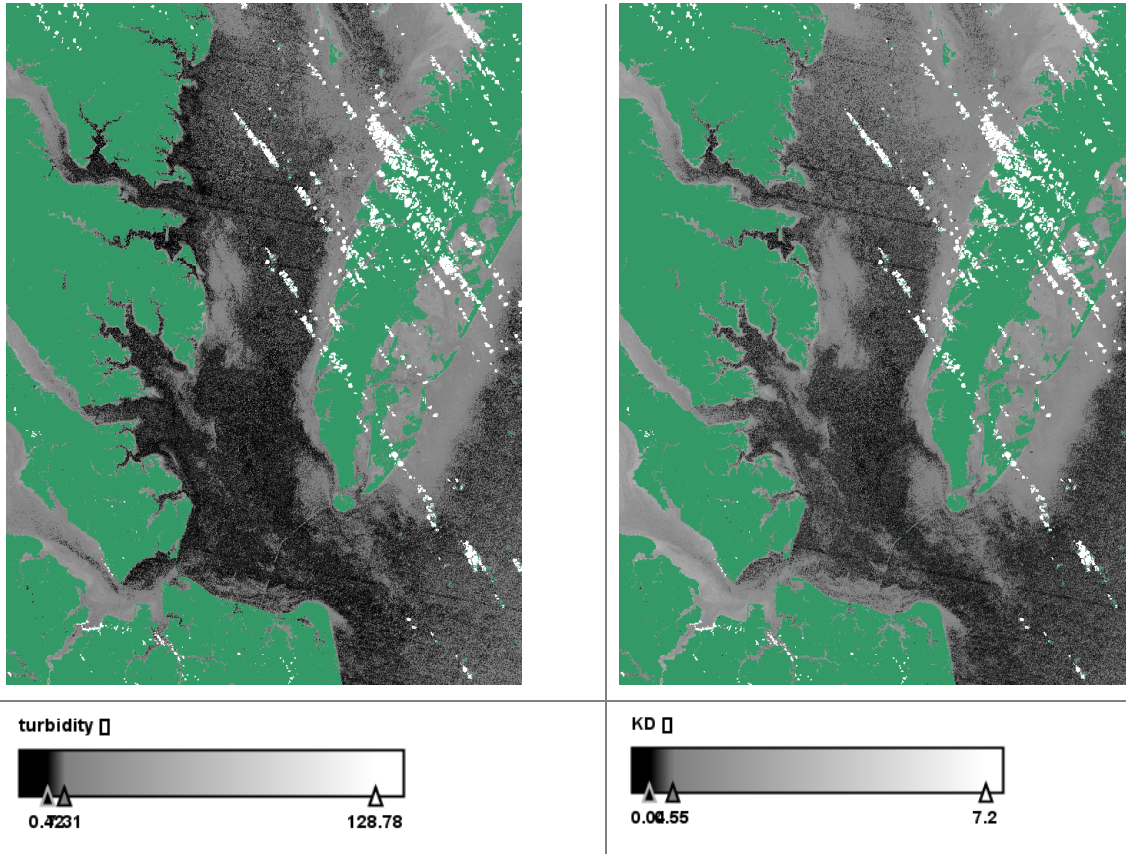


Figure 22 Turbidity and KD values from Landsat 5 (LT50140342008059GN01), colour bar is in log scale.

## 5.3 SPOT 4 Take 5

### 5.3.1 Background and data assessment

Two product levels are provided by CNES (<http://spirit.cnes.fr/take5/#ezpgxczbzury:2>):

- Level 1C : data orthorectified reflectance at the top of the atmosphere
- Level 2A: data orthorectified surface reflectances (after atmospheric correction), along with a mask of clouds and their shadows, and a mask of water and snow

Level 2 data includes three image files and a new folder with the image masks:

- The XML file provides the image metadata, including:
  - Instrument, date and acquisition time
  - Geographic projection, Footprint
  - Solar and Viewing angles at the scene center :
    - Theta\_s : Solar Zenith Angle (0 at zenith);
    - Phi\_s : Solar Azimuth Angle (0 to the North, 90 degrees towards the east)
    - Theta\_v : Viewing Zenith Angle (0 at zenith)
    - Phi\_v : Viewing Azimuth Angle (0 to the North, 90 degrees towards the east)
- Two .TIF files in GeoTiff format that provide surface reflectances, corrected from atmospheric effects, including adjacency effects (ORTHO\_SURF\_CORR\_ENV) and even terrain ef-

fects (ORTHO\_SURF\_CORR\_PENTE). The highest quality product should be ORTHO\_SURF\_CORR\_PENTE, but in some cases, because of insufficient accuracy of the Digital Elevation Model, some artefacts may appear. However, for water surfaces, this is not relevant. These files contain:

- XS1 (0.5-0.59  $\mu\text{m}$ ), XS2 (0.61-0.68  $\mu\text{m}$ ), XS3 (0.78-0.89  $\mu\text{m}$ ) and SWIR (1.58-1.75  $\mu\text{m}$ ) surface reflectances coded as signed 16 bits integers
  - No\_Data value (outside the footprint) is -10000
  - the AOT TIF file provides the estimates of Aerosol Optical Thicknesses (AOT) 16 bits integer
- The mask directory has:
    - A saturated pixels mask \_SAT.TIF (as in Level 1C)
    - A mask of clouds and cloud shadows \_NUA.TIF
    - A water, snow and no\_data mask \_DIV.TIF

The spectrum analysis of one SPOT image on the Chesapeake Bay is shown in Figure 23. Clear (blue and light blue lines, pins 1 and 4) and highly turbid water possibly affected by bottom reflection (yellow and red lines, pins 2 and 7) are easily distinguishable by the different reflectance values in the XS1, 550 nm band. The difference is still high in the red band (XS2, 650nm) and the near-infrared (XS3, 850 nm). Discriminate among degrees of turbidity is more difficult: pins 3 (green line), 5 and 6 have a very similar response; but separation using XS1 and XS2 seems still possible. The band in the red looks like the more useful for discriminating waters that show different colours, so XS-2 is considered as our first band for the following tests; as well as the ratio of the bands green and red, following the logic of the Landsat 5 exercise explained before.

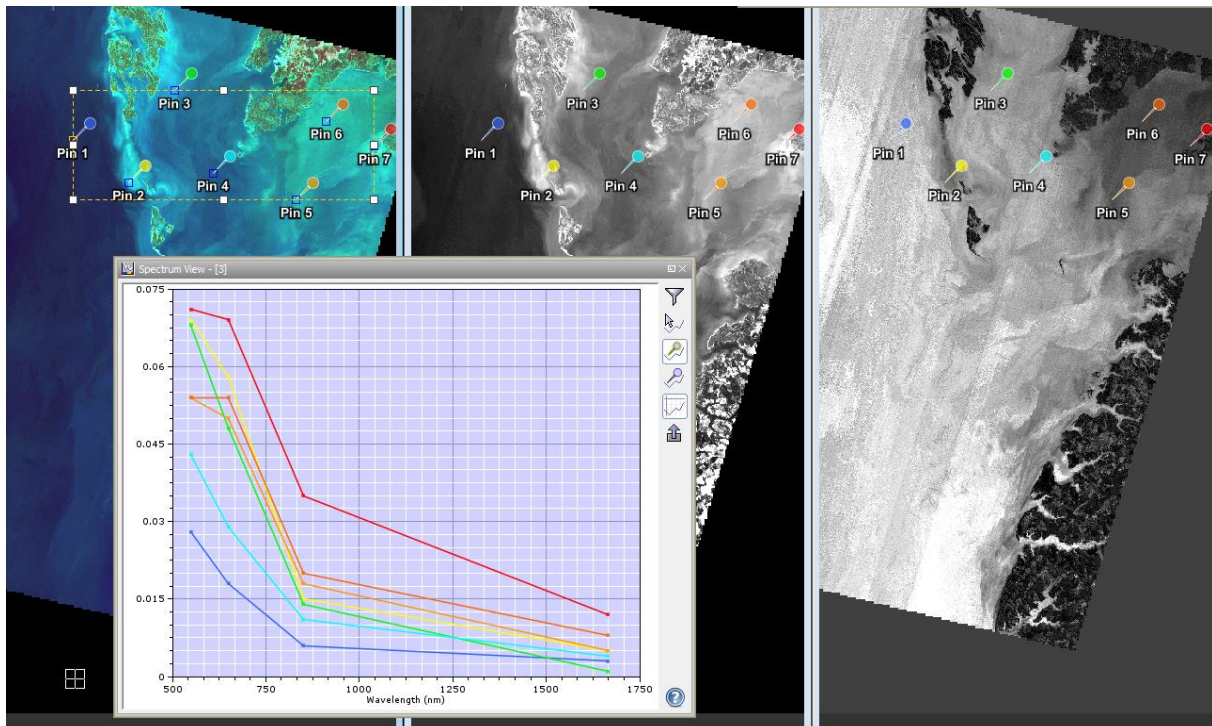
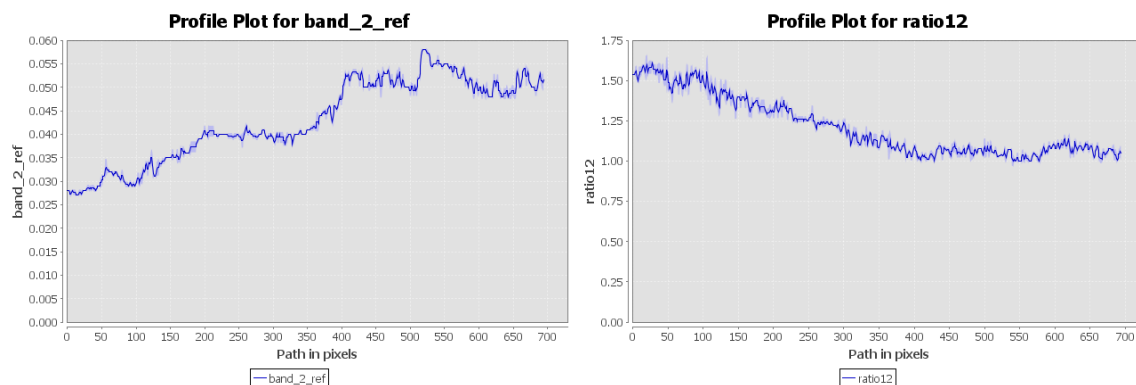
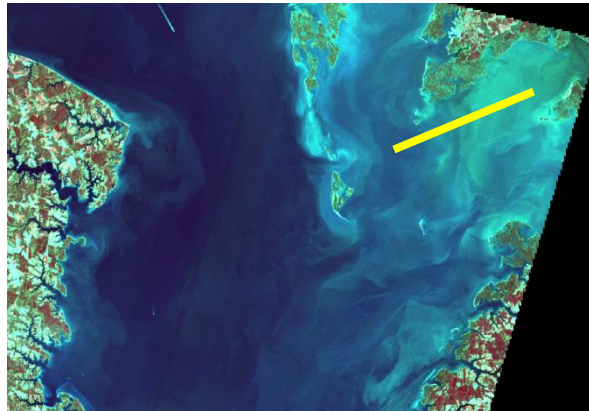


Figure 23 SPOT Spectral behaviour of seven different water colours in the study area (13.03.2013), the spectrum view shows surface reflectances.



**Figure 24** Values in the transect drawn in the image for XS2 and the ratio X1/X2 (direction from southwest to northeast)

### 5.3.2 Methods

Derivation of water quality products from SPOT 4 Take 5 data is done using the ratio of the green/red bands and applying the Nechad approach to the red band. The new bands are then compared with MODIS products: (a) standard MODIS L2 Kd490 product; and (b) the TSM product derived using the empirical TSM calculation from Ondrusek et al. (2012). Results are tested using regression analysis.

#### 5.3.2.1. Ratios (Kd490 and TSM comparisons)

##### 5.3.2.1.1 Kd490 test

A MODIS L2 OC image was downloaded from the NASA Ocean Colour website with the purpose of having a reference of the water quality products. The MODIS and SPOT scenes from the 13 of March 2013 were spatially and geographically collocated. Figure 25 shows a VISAT screenshot with the SPOT image in the upper row as RGB composite, the red band and the ratio X<sub>S1</sub>/X<sub>S2</sub>. The lower row shows MODIS and SPOT, where SPOT was aggregated to 1 km and mapped on MODIS pixel grid. From left to right, the MODIS KD490 (in dark grey invalid pixels), the SPOT red band and the ratio X<sub>S1</sub>/X<sub>S2</sub>. The SPOT data are overlaid with the MODIS land mask to have a reference of the study area.

A few pixels have been selecting using a polyline transect through the Pocomoke Sound, inside the bay and quite close to the coast. This was the only place where there were coincident data between the MODIS KD490 product and the SPOT data. The scatter plot of band KD490 and the green-red ratio is shown in Figure 26. All types of regression have similar coefficients of determination, which could do easier the translation of the ratio values into quantifiable parameters.

There are some pairs of MODIS-SPOT available, but many SPOT images, especially the ones in Korea, are affected heavily but the atmosphere or contain glint contamination (see Table 2 and Table 3).

Table 2 MODIS-SPOT pairs

Chesapeake		Korea	
MODIS	SPOT	MODIS	SPOT
2013-02-06	2013-02-06	-	2013-02-21
2013-02-20	2013-02-21	2013-03-03	2013-03-03
2013-03-13	2013-03-13	-	2013-03-08
2013-04-02	2013-04-02	2013-03-23	2013-03-23
2013-04-26	2013-04-27	2013-04-12	2013-04-12
-	2013-05-02	-	2013-04-22
2013-06-01	2013-06-01	-	2013-04-27
-	2013-06-11	2013-05-02	2013-05-02
2013-06-16	2013-06-16	-	2013-05-07

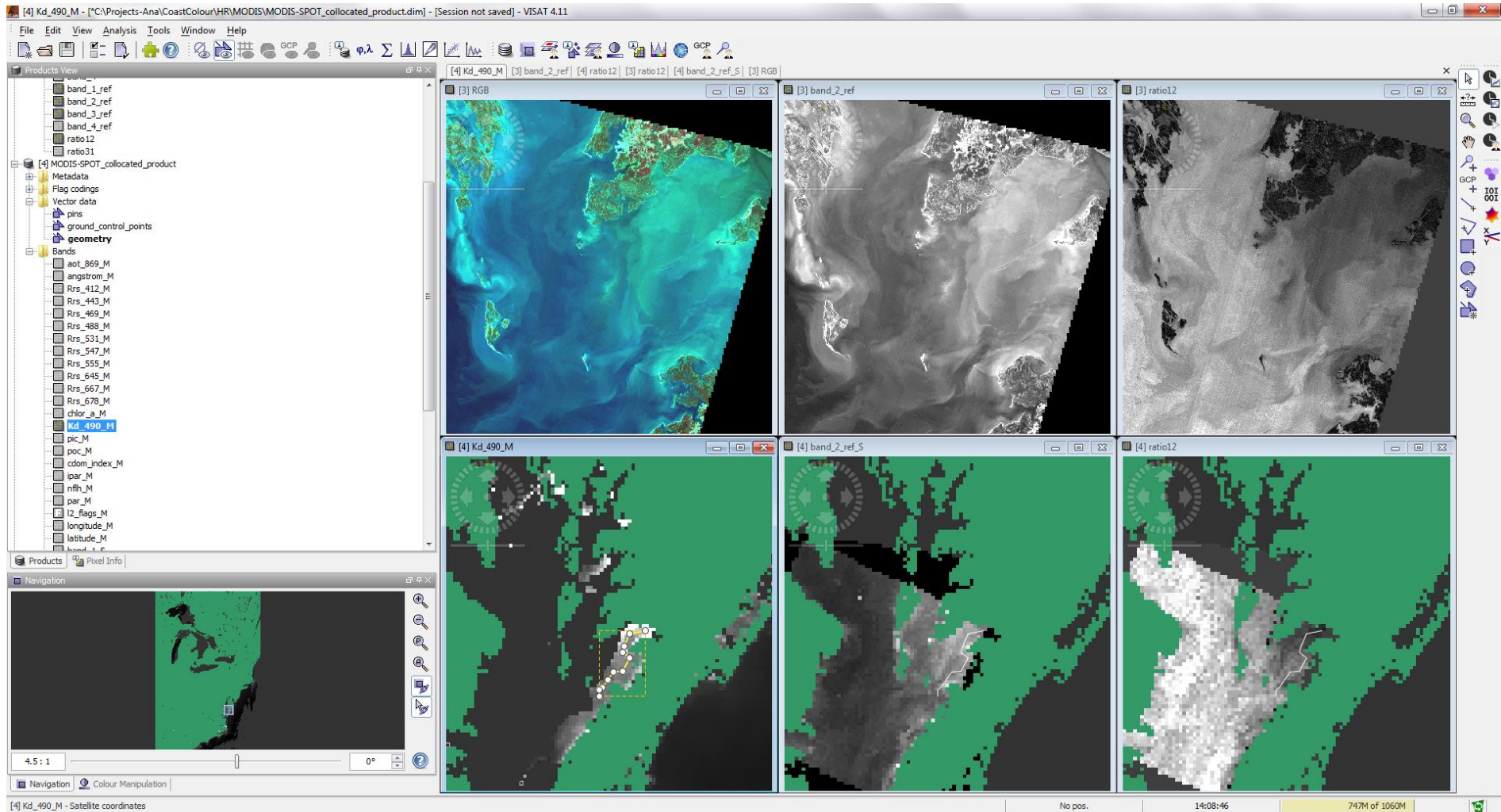


Figure 25 Top: (from left to right) SPOT RGB; band 2 grey scale, ratio XS1/XS2 grey scale. Bottom (from left to right): MODIS-SPOT collocated product MODIS KD490; SPOT XS2 grey scale and ratio XS1/XS2 grey scale (in green the land mask from MODIS products)

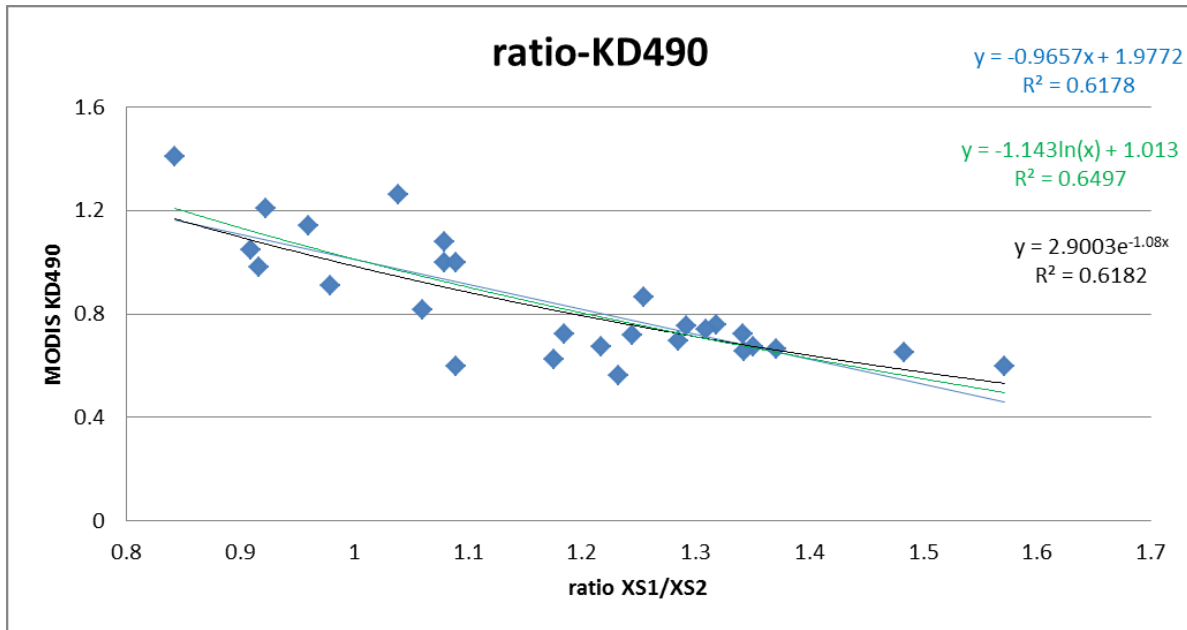


Figure 26 Different regression relations between the SPOT ratio green-red and the MODIS Kd490 values.

#### 5.3.2.2. The Nechad approach

In the paper published by Nechad et al. (2010), a single band algorithm for TSM retrieval based on a reflectance model is developed and calibrated, using seaborne reflectance and TSM measurements in the North Sea area. This algorithm has a simple application to multiple ocean colour sensors, taking into account that is a semi-empirical approach on a determined area and with its particular spatial and temporal variability on specific IOPs.

S -TSM concentration- is estimated from the water leaving reflectance using the following formula:

$$S = \frac{A^P \rho_w}{1 - \rho_w} + B^P \quad \text{Equation 2}$$

Where  $A^P$ ,  $B^P$  and  $C^P$  are calibration coefficients related to the absorption and backscattering properties of the water combined with a simplified reflectance model based on a first order version of the model of Gordon et al. (1988).

The computed calibration factors are given in the paper in form of tables every 2.5 nm for wavelength ranging from 520 to 885 nm. For wavelengths shorter than 600 nm, and in order to avoid the saturation of the TSM model, the value of  $C^P$  was arbitrary set to  $14.49 \cdot 10^{-2}$ . In the paper is recommended not to use this algorithm for wavelengths less than 600 nm. These factors are also computed for MERIS, MODIS and SeaWiFS bands. The  $A^P$  parameter is obtained from non-linear regression analysis using reflectance and TSM in situ data. The parameter  $B^P$  is specific to the measurement errors of the reflectance and TSM data used for calibration; and since there is no reason to suppose that the satellite derived reflectances will have similar errors, this parameter is set to zero for the satellite applications.

The TSM measurements made by Nechad et al. (2010) range from 1.24 gm<sup>-3</sup> to 110.27 gm<sup>-3</sup>, with a standard deviation of 23.35 gm<sup>-3</sup> and average value of 26.16 gm<sup>-3</sup>. The measurements were taken from 2001 to 2006 with a research vessel over the southern North Sea. The Chesapeake Bay TSM concentration ranges measured in 2008 by Ondrusek et al. (2012) -which will be used for comparison purposes- go from 4.50 mgL<sup>-1</sup> to 55.29 mgL<sup>-1</sup>, as it was mentioned in the precedent section.

For an estimation of the TSM concentration using SPOT 4 Take 5, an adaptation of the coefficients to fit the band 2 (610-680nm) is done. After integration of the  $A^p$ ,  $B^p$  and  $C^p$  parameters using the trapezoidal rule, the values for this band are: 281.5773 (gm-3), 2.0543 (gm-3) and  $16.3975 \cdot 10^{-2}$  (dimensionless) respectively. Therefore, the formula used stays like:

$$S = \frac{281.5773 \cdot XS2}{1 - XS2 - 16.3975 \cdot 10^{-2}} \quad \text{Equation 3}$$

This calculation was done on the images from 21 February and 13 March 2013, using the same transects as in the previous section with the results of the fit of the linear regression shown in Figure 27. The linear regression of the data from the Nechad modification of TSM calculation to the XS2 of the SPOT sensor with the MODIS-TSM values extracted by Ondrusek, show a coefficient of determination of 0.56 for these two days and the two transects. The Nechad TSM underestimates the TSM concentration values in the whole range, but at least a trend can be seen with growing values of the SPOT\_TSM with growing values of MODIS\_TSM.

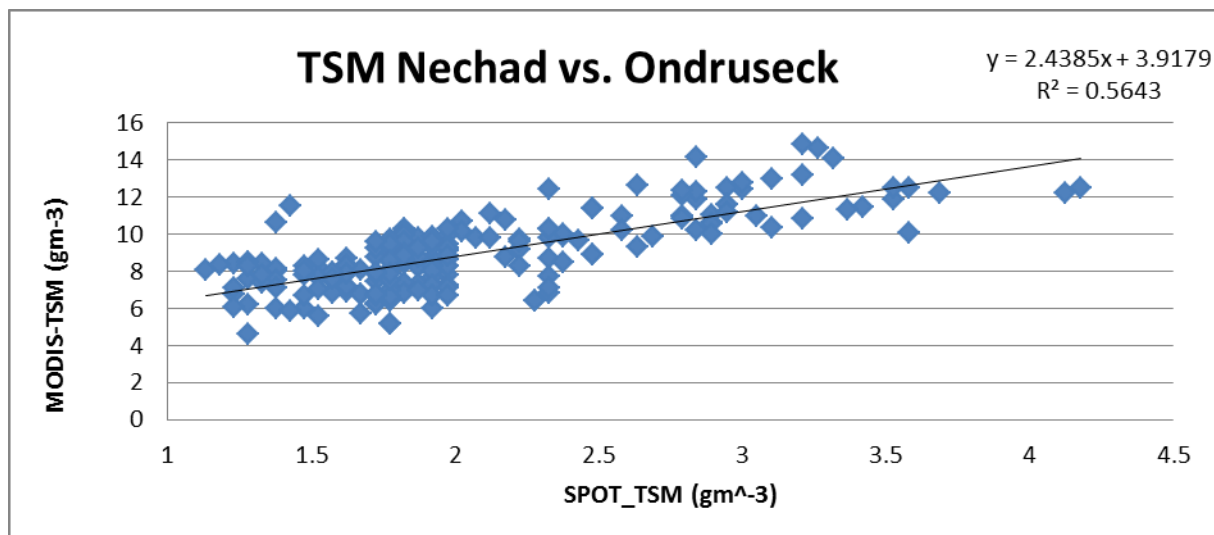


Figure 27 Comparison of the TSM values extracted from the MODIS-TSM product by Ondrusek et al. (2012) and the application of the Nechad formula to SPOT band 2 (610-680 nm)

### 5.3.3 Application examples

#### 5.3.3.1. MODIS Kd490 test for available pairs

From all the possible available MODIS-SPOT pairs for Chesapeake Bay and Korea, only four were suitable for continuing the Kd490 investigation (see in Table 3).

**Table 3 Atmospheric conditions of the MODIS-SPOT pairs**

Chesapeake		Conditions	Korea		Conditions
MODIS	SPOT		MODIS	SPOT	
2013-02-06	2013-02-06	good	-	2013-02-21	
2013-02-20	2013-02-21	good	2013-03-03	2013-03-03	cloudy
2013-03-13	2013-03-13	good	-	2013-03-08	
2013-04-02	2013-04-02	moderate glint	2013-03-23	2013-03-23	cloudy
2013-04-26	2013-04-27	glint	2013-04-12	2013-04-12	good
-	2013-05-02		-	2013-04-22	
2013-06-01	2013-06-01	glint	-	2013-04-27	
-	2013-06-11		2013-05-02	2013-05-02	cloudy
2013-06-16	2013-06-16	glint	-	2013-05-07	

From the pairs, transects with information about the pixel were extracted, and finally only three images/transects had coincident information for Kd490 and SPOT reflectances. The data from these three transects is shown on a scatter plot in Figure 28. The exponential relation is the more appropriate, but the correlation of coefficient looks very low to be significant. We observed that the smallest Kd490 values were all located in Korea. The results for the Korea site are plotted in Figure 29. It can be observed that the linear and exponential regression give similar results, with low coefficients of correlation. A further search in the dataset determined that all the transects are affected by the MODIS straylight flag, and they should not be used to compare with any other product. Unfortunately, this area was the only one with coincident pixels MODIS-SPOT.

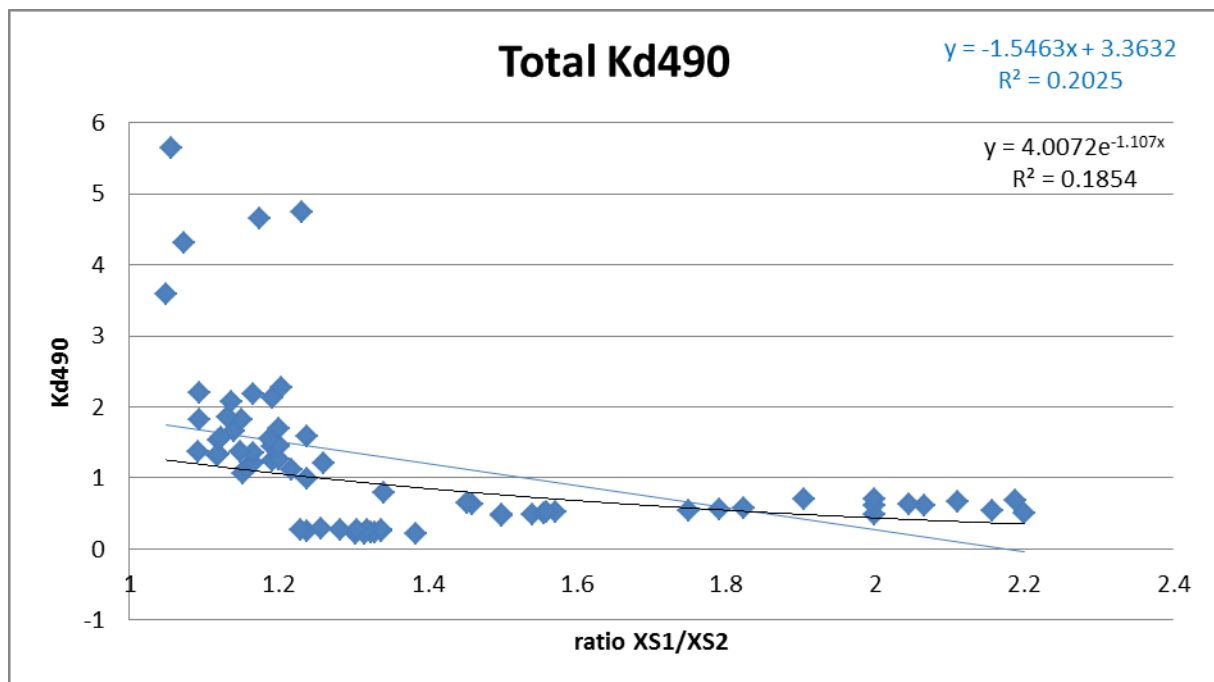


**Figure 28 Chesapeake + Korea, all data**

The match-ups corresponding to the Korea site were then removed from the scatterplot and the statistics improved slightly. Still the correlation looks low, so we also checked the highest Kd490 values, and the one point from the 2013-02-06 with value  $3.5874 \text{ m}^{-1}$  is also flagged as straylight; while the other high values from the 2013-04-02 ( $>4 \text{ m}^{-1}$ ), are flagged as moderate glint. If we remove this high value points from the scatter plot, the polynomial regression seems to work similarly to the plot shown in Figure 26 (see Figure 30). That means, that for this specific dataset -although quite limited- the ratio XS1/XS2 could be used for extracting an equation when the Kd490 values are bigger than  $0.3 \text{ m}^{-1}$  and lower than  $4.0 \text{ m}^{-1}$ .

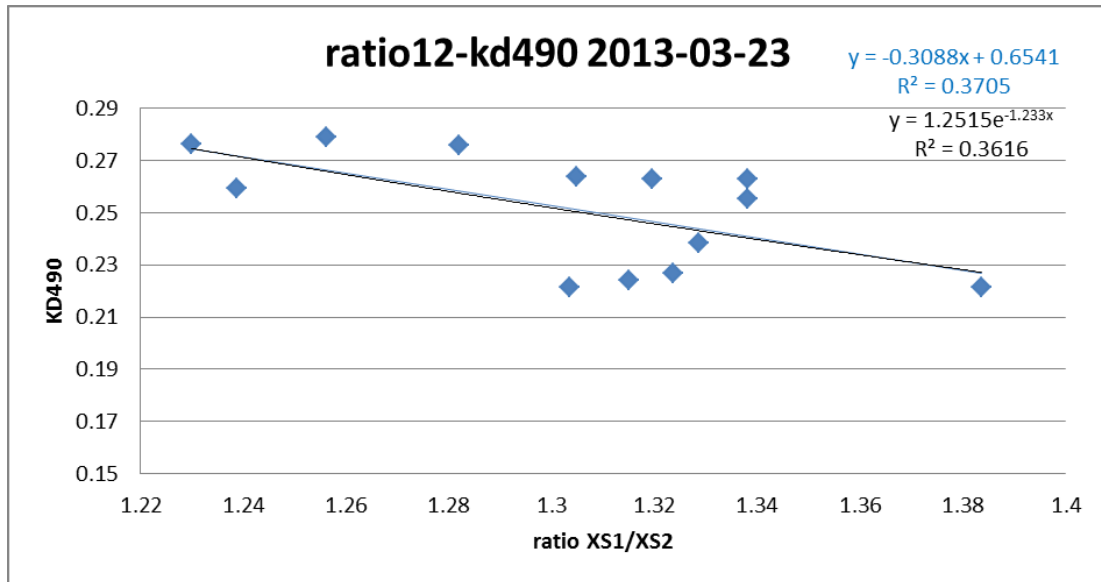


Figure 29 Korea data (all affected by straylight)

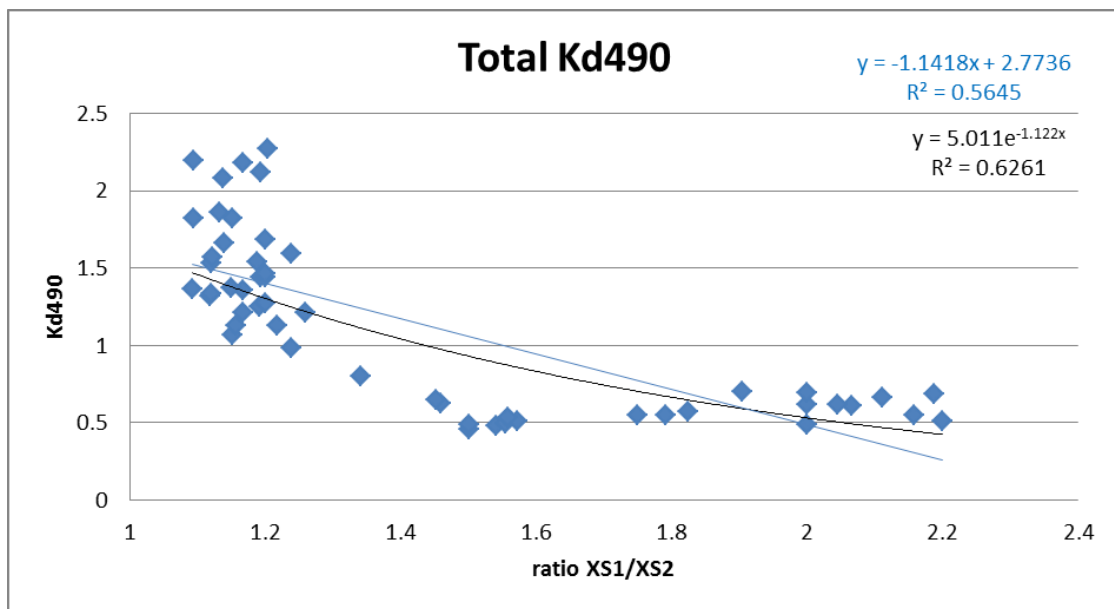


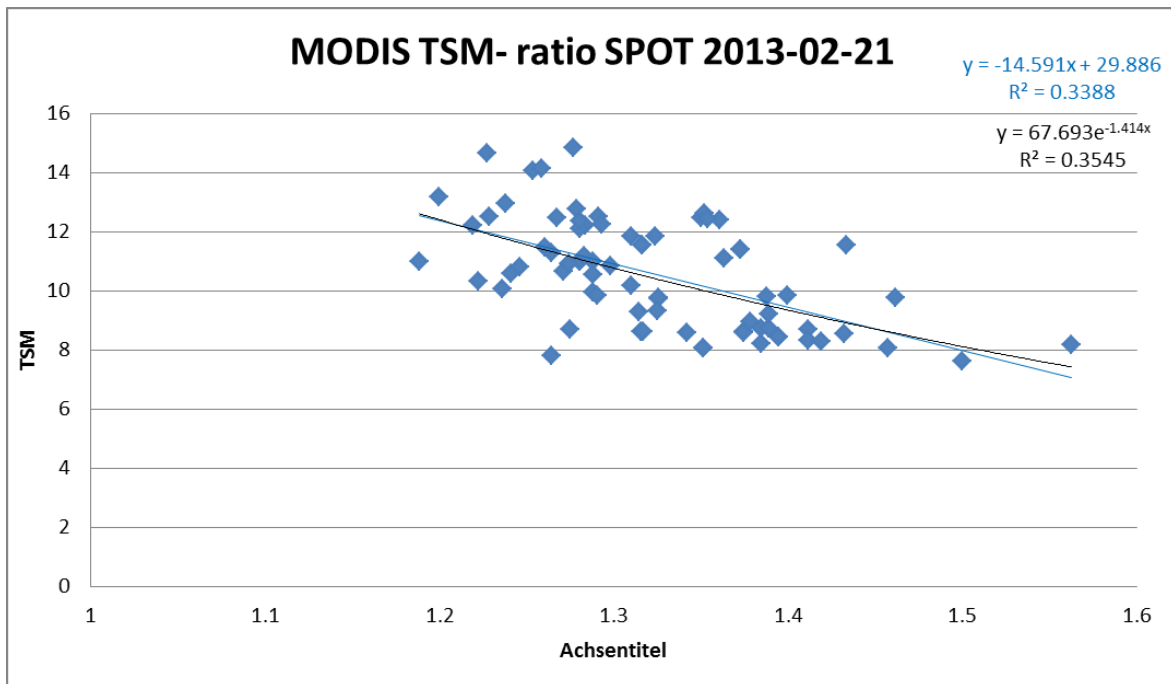
Figure 30 Chesapeake with limitation in Kd490 values ( $>0.3$  and  $< 3.0$ )

### 5.3.3.2. MODIS TSM (250 m) and SPOT ratio comparison

The TSM calculation for the Chesapeake Bay developed for MODIS by Ondrusek et al. (2012) is used to compare with the SPOT ratio products. These authors collected TSM samples on the northern part

of the Chesapeake Bay in three consecutive years (2006-2008) and found ranges of TSM between 4.5 and 55.29 mg/L in the bay area. They also measured in situ water leaving radiance and normalized it. They observed that higher water-leaving radiances were associated with higher TSM concentrations in any range. By comparing in situ normalized water leaving spectra at 645 nm (equivalent to MODIS Band 1) with the measured TSM data for 2008, they established that using a third order polynomial with the y intercept forced through zero fit better than linear regression methods. The linear algorithms exhibited an underestimation of TSM in the higher radiance ranges. The 3<sup>rd</sup> polynomial algorithm reasonably predicted the TSM concentrations over a wide range and they confirmed that is applicable to the whole bay.

The TSM calculated and delivered by the CoastWatch program<sup>2</sup> for the Chesapeake Bay follows this method. A few TSM images corresponding to the SPOT 4 Take 5 passes were downloaded from the database. They correspond to daily values of TSM, calculated with the AQUA-MODIS sensor. The spatial resolution is 250 m and the SPOT images were resized to match that resolution. Transects were drawn to study again the relationship and the results are shown in Figure 31. The relationship of these two parameters seems to be linear, but still the coefficients are higher for the polynomial regression. One of the problems of using the MODIS-TSM product is the lack of a confident flagging. SPOT and MODIS products already contained a land-water and a pixel invalid mask, with NaN as a value, but masks are stored in different files and they should be properly integrated into the collocation product.



<sup>2</sup> [http://coastwatch.Chesapeakebay.noaa.gov/cb\\_tsm\\_current.php](http://coastwatch.Chesapeakebay.noaa.gov/cb_tsm_current.php)

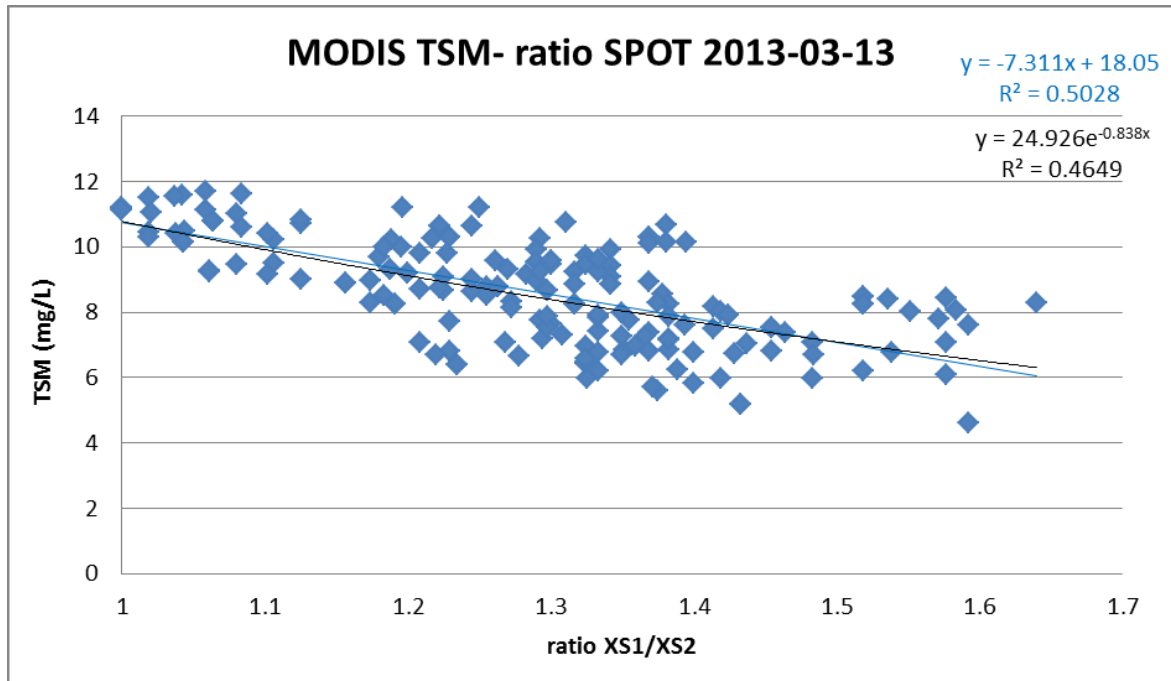


Figure 31 Chesapeake MODIS TSM- ratio XS1/XS2 comparison for the 21 February and the 3 March 2013

5.3.3.3. Comparison of TSM derived from the Nechad approach on MODIS and SPOT for Chesapeake Bay

The approach used by Nechad to calculate the total suspended matter is also use in the standard MODIS scenes to derive TSM. The TSM calculation is done per band (645, 667 and 678 nm) and compare with the SPOT-TSM derived using the same method with the Fehler! Verweisquelle konnte nicht gefunden werden. The coefficients for the MODIS bands were calculated by Nechad and can be seen in Table 4.

Table 4 Coefficients for MODIS central wavelenghts

MODIS bands (nm)	A <sup>P</sup>	C <sup>P</sup> (*10 <sup>-2</sup> )	R <sup>2</sup> %
551	122.01	14.49	53.9
555	112.18	14.49	53.9
645	258.85	16.41	76.8
667	362.09	17.36	79.1
678	400.75	17.74	80.4
748	1768.59	19.88	75.4
858	2846.89	21.12	64.3
869	3031.49	21.16	61.9

SPOT data is resized to 1 km and collocated with the MODIS data for two days: 21 February and 13 March 2013. The TSM bands are calculated over the water leaving reflectance MODIS bands on the 645, 667 and 678 nm. These new TSMs are compared with the SPOT-TSM calculated with the same method. In Figure 32 and Figure 33 are the results for the 21 February 2013. One line is drawn to extract transect data for the four TSM calculations (yellow line). A scatter plot with the results is shown in Figure 33. On a linear regression model the three MODIS-TSMs give similar results when comparing with the SPOT-TSM, being these last measurement slightly higher in magnitude. Unfortunately, the SPOT 4 take 5/MODIS combination data for Korea is very scarce and not plots were derived from them.

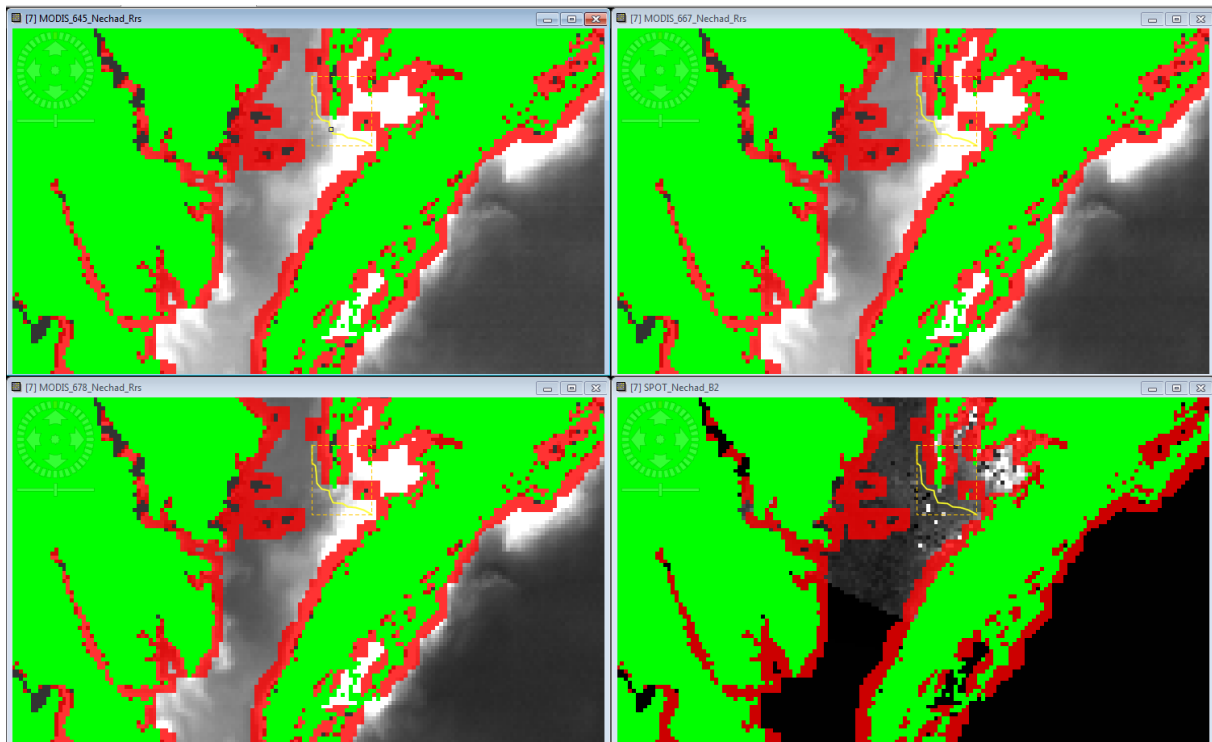


Figure 32 MODIS TSM for bands 645, 667 and 678; SPOT TSM in bottom right corner (2013-02-21). In green the land mask; in red the straylight mask

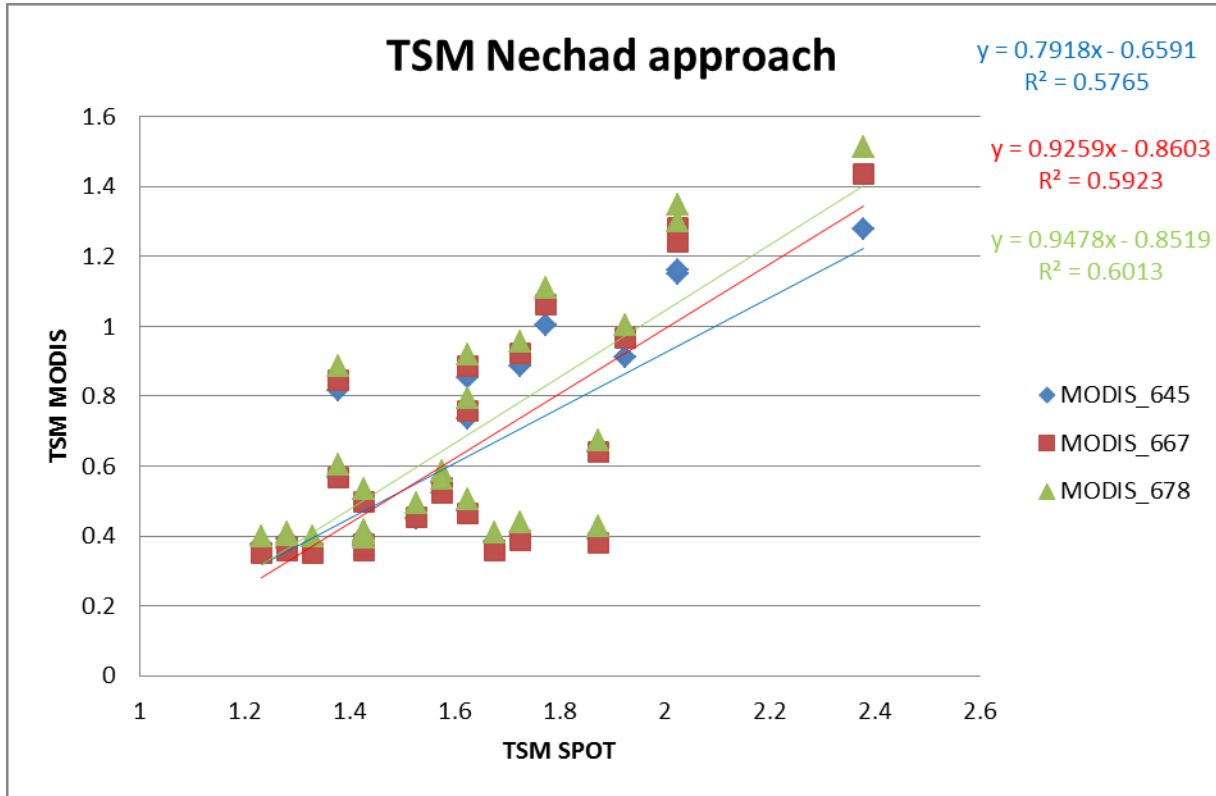


Figure 33 Comparison of SPOT-TSM (x) and the MODIS TSM (y) in bands 645, 667 and 678 nm (blue, red and green respectively) on 2013-02-21

Similar results are shown in Figure 34 and Figure 35 for the 3 March 2013. In this case, all possible coincident pixels are flagged as straylight.

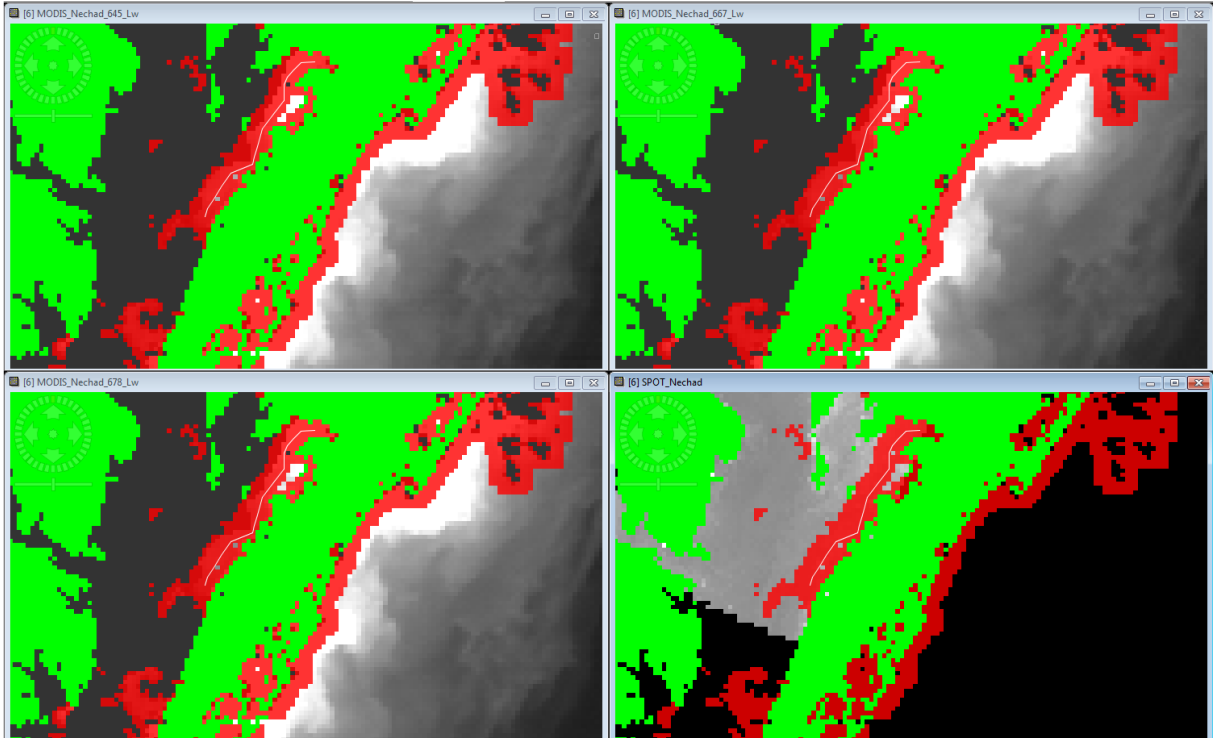


Figure 34 MODIS TSM for bands 645, 667 and 678; SPOT TSM in bottom right corner (2013-03-13). Profile data is flagged as straylight in MODIS. ). In green the land mask; in red the straylight mask

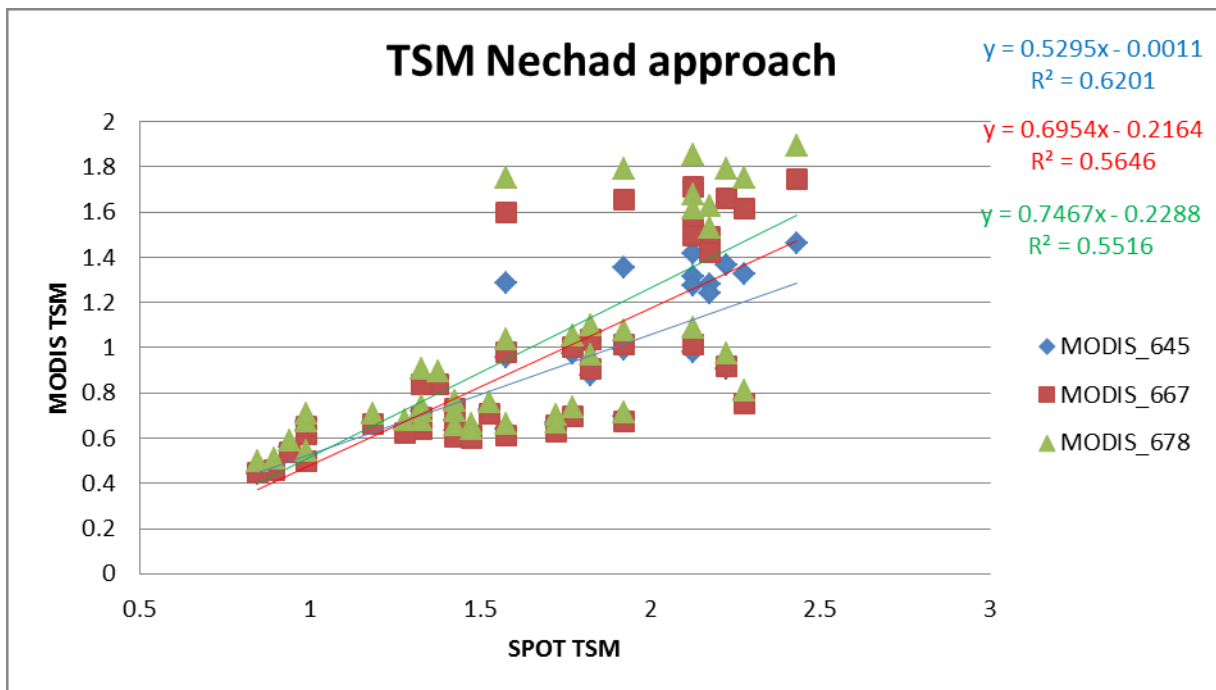


Figure 35 Comparison of SPOT-TSM (x) and the MODIS TSM (y) in bands 645, 667 and 678 nm (blue, red and green respectively) on 2013-03-13

Several TSM products from SPOT imagery using the Nechad approach have been generated for the Chesapeake Bay area. A qualitative comparison of SPOT and MODIS scenes shows that both sensors

	<b>Doc:</b>	Coastcolour-HighRes-ATBD-1.0.doc		
	<b>Date:</b>	25.04.2014		
	<b>Issue:</b>	1	<b>Revision:</b>	0

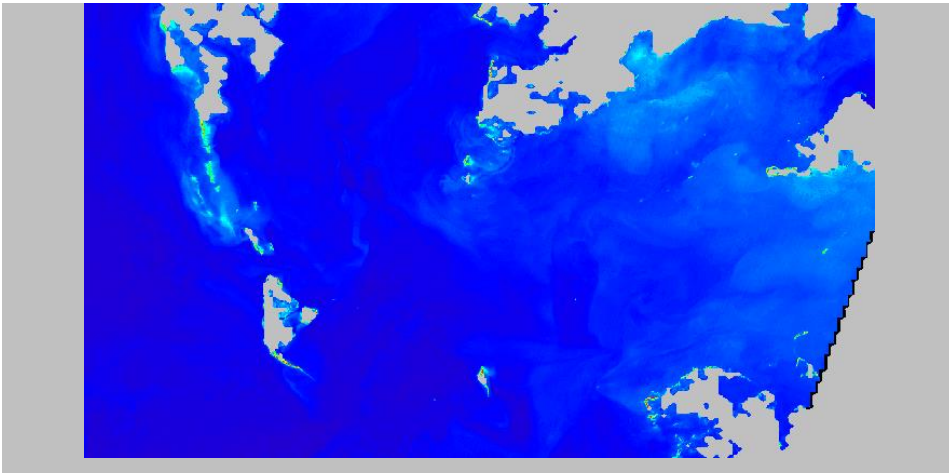
reveal similar patterns. The absolute TSM values are comparable as well, within  $0 > \text{TSM} < 20 \text{ g/m}^3$  (Figure 36, Figure 37, Figure 38).

The SPOT TSM products for all available SPOT 4 Take 5 Chesapeake Bay and Korea site are shown below and can be found on the CoastColour ftp.

2013-02-06 SPOT\_RGB



2013-02-06 SPOT\_TSM\_Nechad (20 m)



2013-02-06 MODIS\_Nechad\_678 (1 km)

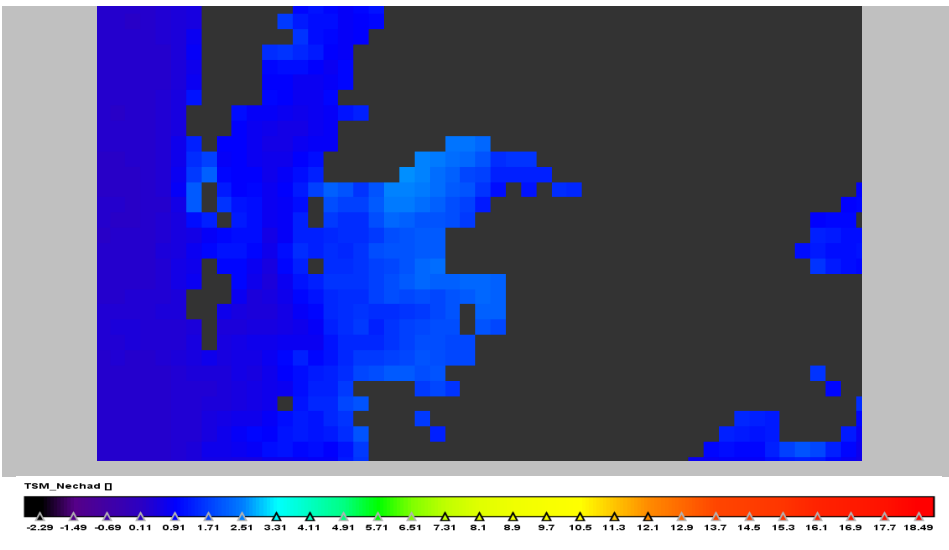
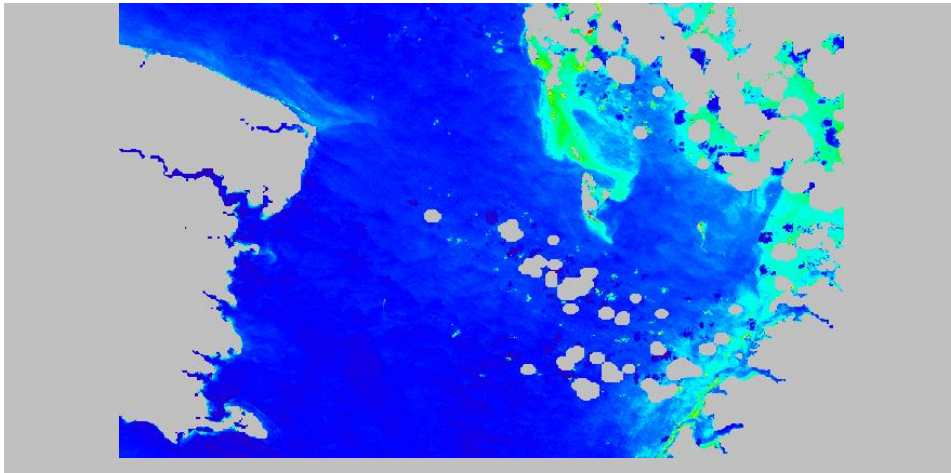


Figure 36 SPOT TSM and MODIS TSM for 2013-02-06: upper image, SPOT RGB composition; middle, SPOT TSM, and bottom, MODIS TSM

2013-02-21 SPOT\_RGB



2013-02-21 SPOT\_TSM\_Nechad (20 m)



2013-02-20 MODIS\_Nechad\_678 (1 km)

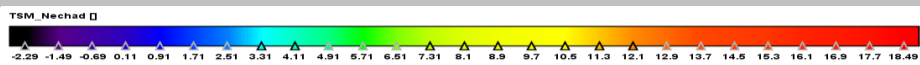
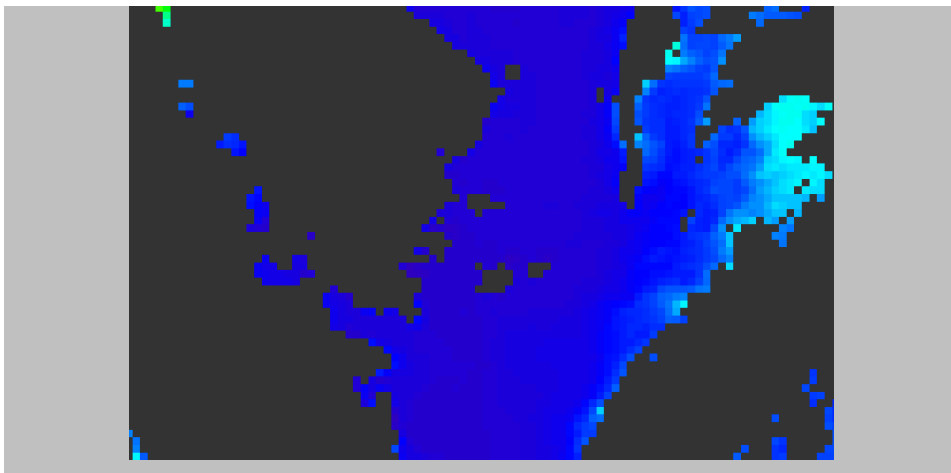
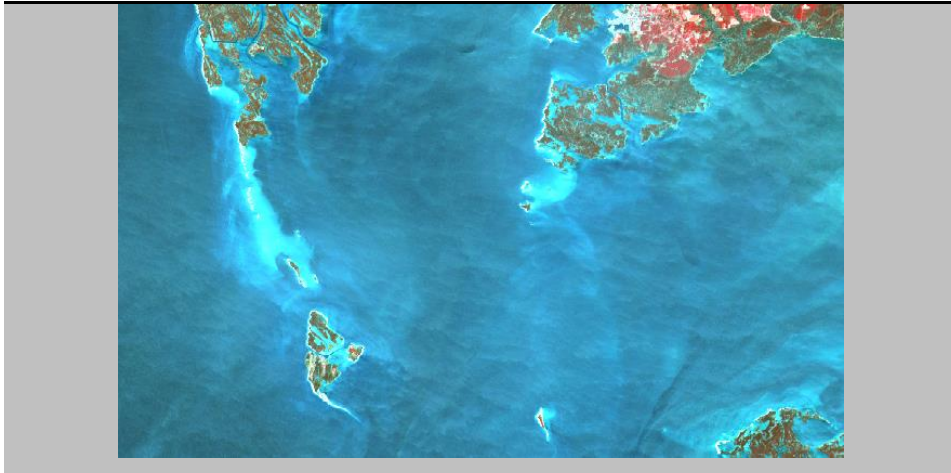
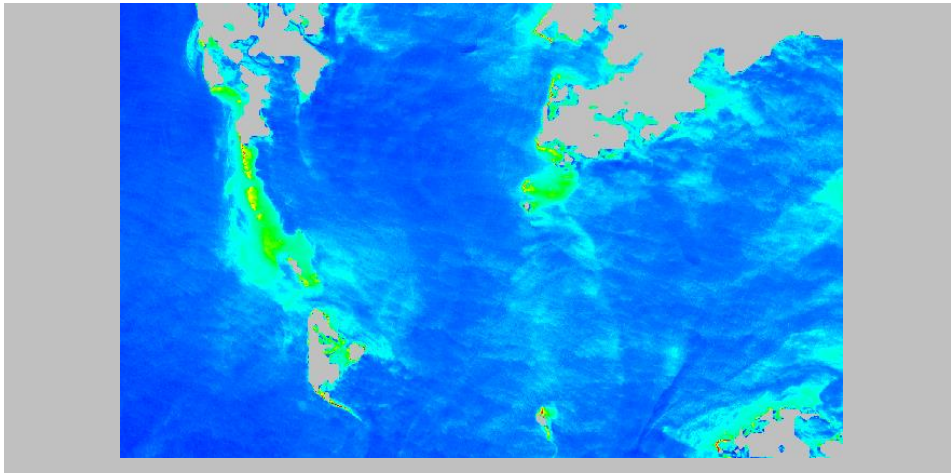


Figure 37 SPOT TSM and MODIS TSM for 2013-02-06: upper image, SPOT RGB composition; middle, SPOT TSM, and bottom, MODIS TSM

2013-04-02 SPOT\_RGB



2013-04-02 SPOT\_TSM\_Nechad (20 m)



2013-04-02 MODIS\_Nechad\_678 (1km)

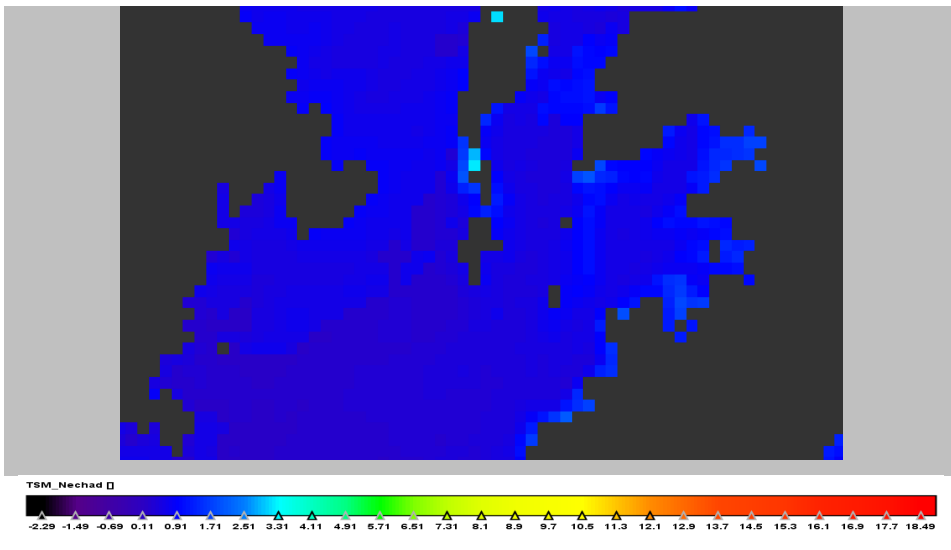


Figure 38 SPOT TSM and MODIS TSM for 2013-02-06: upper image, SPOT RGB composition; middle, SPOT TSM, and bottom, MODIS TSM

## 5.4 Rapid Eye

### 5.4.1 Background

RapidEye is a constellation of 5 identical satellites, providing large earth coverage at a 5m spatial resolution. Revisiting time is daily (off nadir) and every 5.5 days at nadir. A RapidEye data consists of 5 bands, one in the blue, and in the green range, two in the red and one in the near-infrared (Table 5) -ranging from 440nm to 850nm-.

Table 5 RapidEye bands and spectral range

Band #	Name	Spectral Range (nm)
1	Blue	440 - 510
2	Green	520 - 590
3	Red	630 - 685
4	Red Edge	690 - 730
5	Near-Infrared	760 - 850

### 5.4.2 Converting RapidEye radiances into reflectances

To compare RapidEye data with MERIS reflectances, several steps should be taken first, since the data of the RapidEye image pixels represent absolute calibrated radiance values for non atmospheric corrected images. The first step is to take the radiometric scale factor into account, in order to convert the original value (OV) of each pixel into TOA radiances (RAD) in  $W \cdot m^{-2} \cdot sr^{-1} \cdot \mu m^{-1}$  (Equation 4):

$$RAD(i) = OV(i) * radiometricScaleFactor(i) \quad \text{Equation 4}$$

The radiometric scale factor for each band can be found in the image XML metadata file under the band specific metadata.

In order to derive reflectances from the calculated TOA radiances, the transformation equation (Equation 5) provided by RapidEye has to be applied, taking into consideration only the sun distance and the geometry of the incoming solar radiation.

$$REF(i) = RAD(i) \frac{\pi * SunDist^2}{EAI(i) * \cos(SolarZenith)} \quad \text{Equation 5}$$

where:

- i: Number of the spectral band
- REF: reflectance value
- RAD: Radiance value
- SunDist: Earth-Sun Distance at the day of acquisition in Astronomical Units (Note: This value is not fix, it varies between 0.983 289 8912 AU and 1.016 710 3335 AU and has to be calculated for the image acquisition point in time.
- EAI: Exo-Atmospheric Irradiance
- SolarZenit: Solar Zenith angle in degrees (= 90° - sun elevation)

	<b>Doc:</b>	Coastcolour-HighRes-ATBD-1.0.doc		
	<b>Date:</b>	25.04.2014		
	<b>Issue:</b>	1	<b>Revision:</b>	0

For RapidEye the EAI values for the 5 bands are:

- Blue: 1997.8 W.m<sup>-2</sup>μm<sup>-1</sup>
- Green: 1863.5 W.m<sup>-2</sup>μm<sup>-1</sup>
- Red: 1560.4 W.m<sup>-2</sup>μm<sup>-1</sup>
- Red Edge: 1395.0 W.m<sup>-2</sup>μm<sup>-1</sup>
- Near-Infrared: 1124.4 W.m<sup>-2</sup>μm<sup>-1</sup>

This results in TOA reflectances, still not atmospheric corrected; because of the few spectral bands, their spectral width and spectral location, it is not possible to apply a marine atmospheric correction. One possibility is to use atmospheric correction parameters from an appropriate ocean colour sensor, coincident (more or less) with the RapidEye overpass and at good spatial resolution (i.e. only MERIS is a candidate): remove the path and transmittance information, which would be provided by the MERIS image ( Equation 6):

$$REF(atmcorr)(i) = REF(i) - path(i) * Transmittance(i) \quad \text{Equation 6}$$

However, SPOT 4 TAKE 5 experiment took place after the demise of ENVISAT and this conversion from TOA to reflectances was not possible for the dataset used in this study.

For the two study areas, Rapid Eye data covers a small portion of the regions and very close to the coast. This make difficult to find pair of MODIS data with coincident valid pixels, due to the big gap on resolution differences. The footprint of the Rapid Eye scenes in Chesapeake Bay can be seen on the inset on the upper right corner of Figure 39.



**Figure 39 Chesapeake Bay Rapid Eye RGB scene**

The footprint of Rapid Eye scenes in Korea can be seen on the inset on the upper left corner of Figure 40.



Figure 40 Korea Rapid Eye RGB scene

In the Table 6 and Table 7, there are two lists with the Rapid Eye data available in these two areas and their atmospheric conditions.

Table 6 Conditions of Rapid Eye data in the Chesapeake Bay

Chesapeake bay	Condition
1856410_2013-02-06_RE1_3A_154140	good
1856410_2013-02-11_RE1_3A_154520	cloudy
1856410_2013-02-16_RE2_3A_154075	cloudy
1856410_2013-02-21_RE2_3A_156372	good
1856410_2013-02-26_RE2_3A_156766	cloudy
1856410_2013-03-03_RE2_3A_156984	cloudy
1856410_2013-03-08_RE3_3A_157780	cloudy

1856410_2013-03-13_RE3_3A_158131	quite good
1856410_2013-03-18_RE3_3A_158313	cloudy
1856410_2013-03-23_RE3_3A_158700	good
1856410_2013-03-28_RE4_3A_156495	cloudy
1856410_2013-04-02_RE4_3A_159422	good
1856410_2013-04-07_RE4_3A_160200	good
1856410_2013-04-12_RE5_3A_160205	cloudy
1856410_2013-04-17_RE5_3A_160356	foggy
1856410_2013-04-22_RE5_3A_160836	cloudy and incomplete
1856410_2013-04-27_RE5_3A_160977	sun glint
1856410_2013-05-07_RE1_3A_161699	cloudy
1856410_2013-05-12_RE1_3A_162077	cloudy
1856410_2013-05-17_RE1_3A_162376	cloudy
1856410_2013-05-22_RE1_3A_162699	ok, some clouds
1856410_2013-05-27_RE2_3A_162297	sun glint
1856410_2013-06-01_RE2_3A_163270	sun glint
1856410_2013-06-06_RE2_3A_165357	cloudy
1856410_2013-06-11_RE2_3A_164098	cloudy
1856410_2013-06-16_RE3_3A_164274	sun glint

Table 7 Conditions of Rapid Eye data in the Chesapeake Bay

Korea	
5255304_2013-02-06_RE3_3A_152950	cloudy
5255304_2013-02-06_RE3_3A_154163	cloudy
5255304_2013-02-11_RE3_3A_154060	good
5255304_2013-02-11_RE3_3A_154060	good
5255304_2013-02-21_RE4_3A_154171	good
5255304_2013-02-26_RE4_3A_156767	cloudy
5255304_2013-03-03_RE4_3A_156425	cloudy
5255304_2013-03-08_RE4_3A_156439	noisy
5255304_2013-03-13_RE5_3A_156454	cloudy
5255304_2013-03-18_RE5_3A_156468	cloudy
5255304_2013-03-23_RE5_3A_156482	good
5255304_2013-03-28_RE1_3A_156496	good, some glint
5255304_2013-04-02_RE1_3A_159084	cloudy
5255304_2013-04-07_RE1_3A_159099	cloudy
5255304_2013-04-12_RE1_3A_159113	good
5255304_2013-04-17_RE1_3A_159567	cloudy
5255304_2013-04-27_RE2_3A_159595	cloudy
5255304_2013-05-07_RE3_3A_160878	good

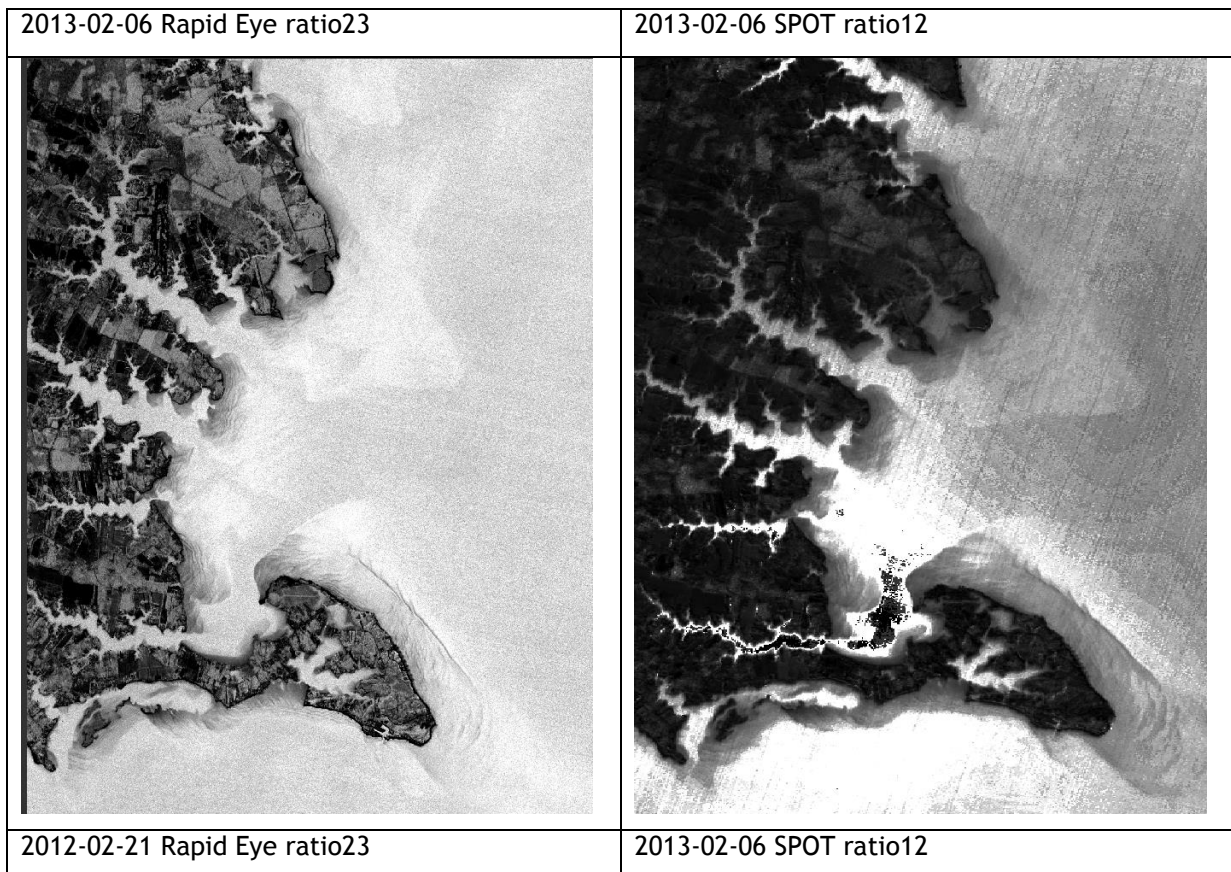
5255304_2013-05-12_RE3_3A_160892	good, some glint
5255304_2013-05-17_RE3_3A_162375	cloudy
5255304_2013-05-22_RE3_3A_162264	good
5255304_2013-06-16_RE5_3A_163258	good

### 5.4.3 Method

The main disadvantage of being forced to use TOA radiances instead of marine reflectances is that the Nechad approach is not applicable with these set of Rapid Eye data. Another disadvantage of this particular dataset is that the few images that are not cloudy do not contain turbid waters. In order to have an idea of what Rapid Eye can offer, the ratio green/red was calculated in four image pairs Rapid Eye-SPOT, to see if at least we could observed the same patters in the water. These patterns are visible in both type of data

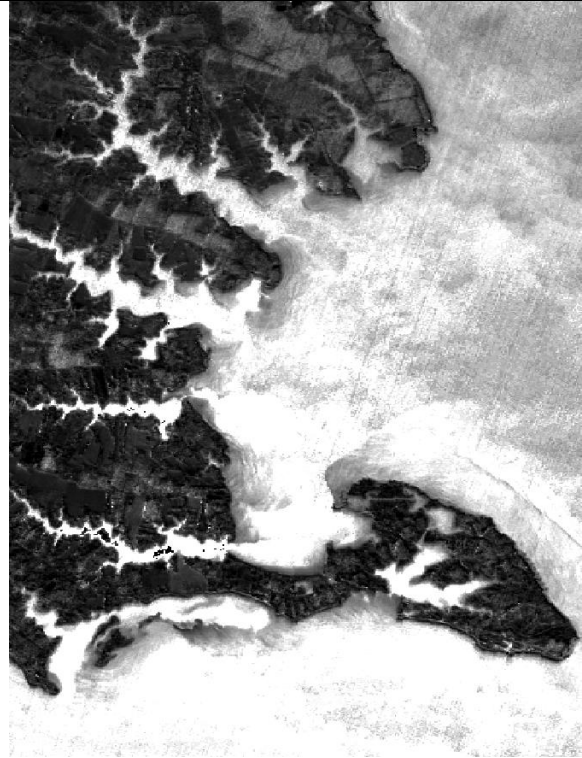
### 5.4.4 Application examples

Comparison of four Rapid Eye-SPOT pairs ratio green/red in shown in Figure 41.





2013-03-13 Rapid Eye ratio23



2013-02-06 SPOT ratio12



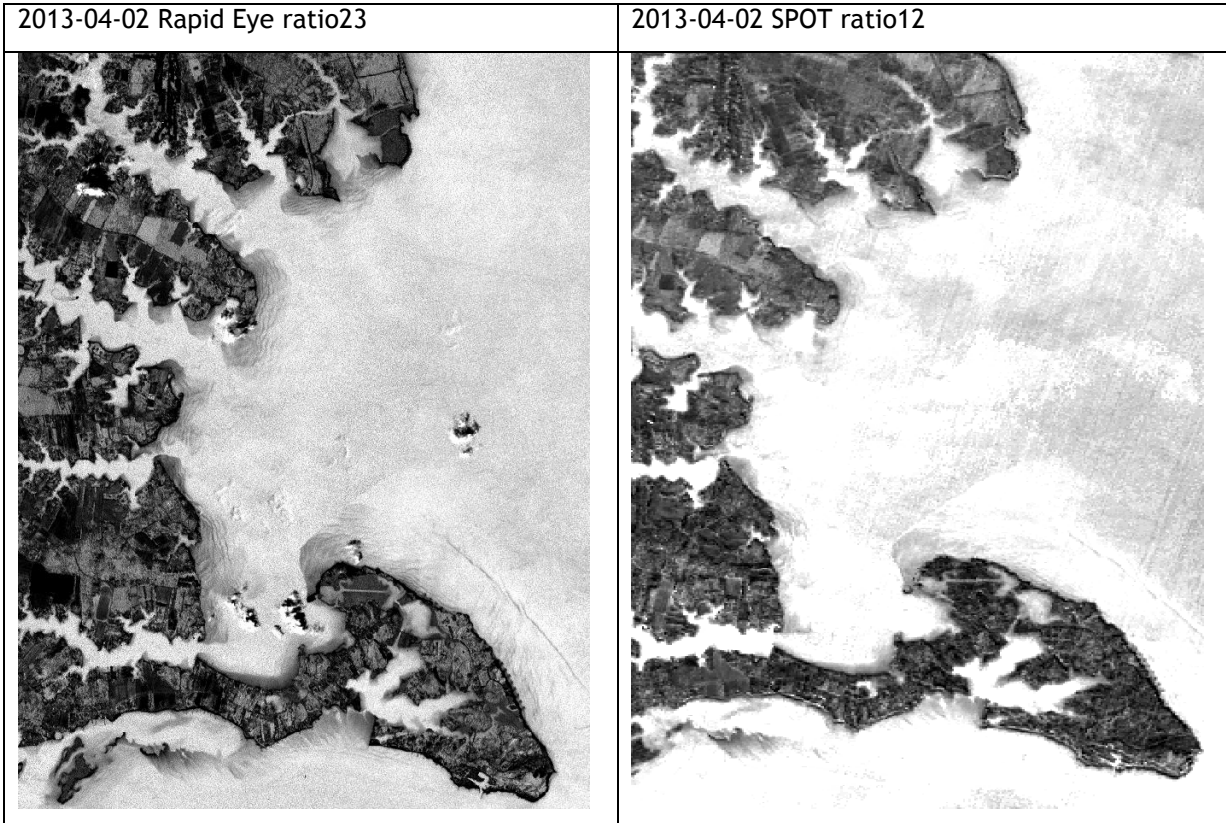


Figure 41 Rapid Eye green/red ratio vs SPOT green/red ratio in Chesapeake Bay

## 6 ERRORS AND LIMITATIONS

One of the limitations when facing the challenge of extracting valuable ocean colour information from high resolution sensors, is the lack of in situ data available to generate match-ups with the satellite overpasses. This fact led to a re-orientation of the methodology, which was planned to be based on empirical approaches, following the literature reviewed on Landsat and SPOT. In terms of validation, the lack of verifiable in situ information becomes a major disadvantage and complicates the calculation of quantitative TSM or CHL concentrations.

In other to overcome this difficulty, several approaches used in the literature were tested, excluding the calibration steps, and using comparable data from other remote sensing sources. Good atmospherically corrected data are then needed, because the products should be the closer the better in terms of quality. This leads to a different type of problems and error generators, like the results of the atmospheric correction approaches used and the method to flag invalid data (pixel identification and cloud screening). Unfortunately, the cloud screening of the HR data used in this study is quite deficient and there are some problems not quite yet assessed, like the glint and the adjacency effect (besides the haze and the mixed-pixel cases). Bottom reflection is also visible in most of the cases, and it is highly recommended to be accounted for when working with high resolution imagery (see Figure 39 and Figure 40).

The viewing differences conditions and sensor design can also introduce problems when comparing data from different sensors. For instance, the view zenith angles are frequently quite large in MODIS, and this introduces geometric distortion in the images. This could cause a spatial mismatch with the nadir-view of SPOT and Landsat images. The spatial mismatch introduces errors especially due to the resolution difference of the sensors. Furthermore, due to the scanning system of MODIS, the edge of swath pixels have a much larger footprint than the central pixels (“bow-tie” effect).

	<b>Doc:</b>	Coastcolour-HighRes-ATBD-1.0.doc		
	<b>Date:</b>	25.04.2014		
	<b>Issue:</b>	1	<b>Revision:</b>	0

In addition to the spatial errors, the time difference of the images compared can also cause significant differences in surface TSM concentrations. These differences exist even when comparing the same images with adjacent swaths and separated by minimum time (Vanhellemont & Ruddick, 2014).

## 7 REFERENCES

Dekker, A. G., Vos, R. J., & Peters, S. W. M. (2001). Comparison of remote sensing data, model results and in situ data for total suspended matter (TSM) in the southern Frisian lakes, *The Science of the Total Environment* 268, 197-214.

Doxaran, D., Froidefond, J.-M., & Castaing, P. (2002). A reflectance band ratio used to estimate suspended matter concentrations in sediment-dominated coastal waters. *International Journal of Remote Sensing*, 23(23), 5079-5085. doi:10.1080/0143116021000009912

Doxaran, D., Froidefond, J., Lavender, S., & Castaing, P. (2002). Spectral signature of highly turbid waters Application with SPOT data to quantify suspended particulate matter concentrations. *Remote Sensing of Environment*, 81, 149 - 161.

Kallio, K., Attila, J., Härmä, P., Koponen, S., Pulliainen, J., Hyytiäinen, U.-M., & Pyhälähti, T. (2008). Landsat ETM+ images in the estimation of seasonal lake water quality in boreal river basins. *Environmental Management*, 42(3), 511-22. doi:10.1007/s00267-008-9146-y

Ma, R., & Dai, J. (2005). Investigation of chlorophyll-a and total suspended matter concentrations using Landsat ETM and field spectral measurement in Taihu Lake, China. *International Journal of Remote Sensing*, 26(13), 2779-2795. doi:10.1080/01431160512331326648

Nechad B., Ruddick, K.G. and Park Y. (2010) Calibration and validation of a generic multisensor algorithm for mapping of total suspended matter in turbid waters. *Remote Sensing of the environment* 114, 854-866

Ondrusek, M., Stengel, E., Kinkade, C. S., Vogel, R. L., Keegstra, P., Hunter, C., & Kim, C. (2012). The development of a new optical total suspended matter algorithm for the Chesapeake Bay. *Remote Sensing of Environment*, 119, 243-254. doi:10.1016/j.rse.2011.12.018

Ruddick, K. G., De Cauwer, V., Park, Y.-J., & Moore, G. (2006). Seaborne measurements of near infrared water-leaving reflectance: The similarity spectrum for turbid waters. *Limnology and Oceanography*, 51(2), 1167-1179. doi:10.4319/lo.2006.51.2.1167

Tebbs, E. J., Remedios, J. J., & Harper, D. M. (2013). Remote sensing of chlorophyll-a as a measure of cyanobacterial biomass in Lake Bogoria, a hypertrophic, saline-alkaline, flamingo lake, using Landsat ETM+. *Remote Sensing of Environment*, 135, 92-106. doi:10.1016/j.rse.2013.03.024

Vanhellemont, Q., & Ruddick, K. (2014). Turbid wakes associated with offshore wind turbines observed with Landsat 8. *Remote Sensing of Environment*, 145, 105-115. doi:10.1016/j.rse.2014.01.009

Wang, J., Lu, X. X., Liew, S. C., & Zhou, Y. (2009). Retrieval of suspended sediment concentrations in large turbid rivers using Landsat ETM + : an example from the Yangtze River , China, 1092(March), 1082-1092. doi:10.1002/esp

	<b>Doc:</b>	Coastcolour-HighRes-ATBD-1.0.doc		
	<b>Date:</b>	25.04.2014		
	<b>Issue:</b>	1	<b>Revision:</b>	0

## 8 ACRONYMS AND ABBREVIATIONS

AATSR	Advance Along Track Scanning Radiometer
AC	Atmospheric Correction
AMORGOS	Accurate MERIS ortho-rectified geolocation operational software
ANN	Artificial neural network
AOI	Area of interest
AOP	Apparent optical properties
API	Application Programming Interface
ATBD	Algorithm theoretical basis document
BC	Brockmann Consult
BEAM	Basic Envisat AATSR and MERIS toolbox
BOA	Bottom of Atmosphere
BRF	Bidirectional Reflectance Factor
CC	CostColour
CDOM	Coloured dissolved organic matter
CEOS	Committee on Earth Observation Satellites
Chl	Chlorophyll
ChloroGIN	Chlorophyll Global Integrated Network
CO	Centre of Oceanography of the University Lisbon
CSIR	Council for Scientific and Industrial Research
CSIRO	Commonwealth Scientific and Industrial Research Organisation
CZCS	Coastal Zone Colour Scanner
DDS	ESA's satellite data distribution system
DEL	Delivery
DJF	Design justification file
DPM	Detailed Processing Model
DPQR	Demonstration products and qualification report
DQWG	Data quality working group
DUE	Data User Element of the ESA Earth Observation Envelope Programme
ECSS	European Co-operation for Space Standardisation
EE	Earth Explorer (Mission)
ENVISAT	Environmental Satellite ( <a href="http://envisat.esa.int">http://envisat.esa.int</a> )
EO	Earth observation
EOLI	ESA Earth Observation Link
ERS	European Remote Sensing satellite
ESA	European Space Agency
ESRIN	European Space Research Institute ( <a href="http://www.esa.it/export/esaCP/index.html">http://www.esa.it/export/esaCP/index.html</a> )
FFH	Flora Fauna Habitat Directive
FR	Full resolution (300m resolution MERIS products)
FRS	Full resolution full swath
FTP	File transfer protocol
FLH	Fluorescence Line Height
fWNN	forward artificial neural network
GEO	Group on Earth Observations
GEOSS	Global Earth Observation System of Systems
GIOP	Generic IOP algorithm
GMES	Global Monitoring for Environment and Security

	<b>Doc:</b>	Coastcolour-HighRes-ATBD-1.0.doc		
	<b>Date:</b>	25.04.2014		
	<b>Issue:</b>	1	<b>Revision:</b>	0

GOCI	Geostationary Ocean Color Imager
HAB	Harmful Algal Bloom
ICOL	Improve Contrast between Ocean and Land
IDE	Integrated development environment
IGBP	Geosphere Biosphere Program
INPE	National Institute for Space Research
IOCCG	International Ocean Colour Coordinating Group
IOP	Inherent optical properties
IPF	Instrument Processing Facility
ITT	Invitation to tender
IVM	Institute of Environmental Studies
JAI	Java advanced imaging
JIO	Java image input/output
JRC	Joint Research Centre
Kd(490)	Diffuse absorption coefficient at 490 nm
KO	Project kick-off
KORDI	Korea Ocean Satellite Center
L1, L2	Level 1, Level 2
L1P	A pre-processed version of the standard Level-1 data products.
L2R	Advanced atmospherically corrected L1P data
LISE	University of the Littoral Opal Coast
LOICZ	Land Ocean Interaction in the Coastal Zone
LTO	Linear tape open
LUT	Look Up Table
MEGS	MERIS Ground Segment Data Processing Prototype
MERCI	MERIS Catalogue and Inventory
MERIS	Medium Resolution Imaging Spectrometer (ESA instrument)
MODIS	Moderate Resolution Imaging Spectrometer (NASA instrument)
MUMM	Management Unit of the North Sea Mathematical Models
NASA	National Aeronautics and Space Administration
NIR	Near InfraRed
NRT	Near-real time
OCM	Ocean Colour Monitor
OLCI	Ocean and Land Colour Instrument
OSSD	Open Source Software Development
PAR	Photosynthetically active radiation
PM	Progress meeting
PML	Plymouth Marine Laboratory
POGO	Partnership for Observation of the Global Oceans
PUG	Product User Guide
Q4	4th quarter of the year (October-December)
QA4EO	Quality Assurance Framework for Earth Observation data
QAA	quasi-analytical algorithm
RB	Requirements baseline
RD	Reference document
REVAMP	Regional Validation of MERIS chlorophyll Product
RID	Review item discrepancy
RH	relative humidity
ROI IOCCG	Regional bio-Optical algorithms Initiative

	<b>Doc:</b>	Coastcolour-HighRes-ATBD-1.0.doc		
	<b>Date:</b>	25.04.2014		
	<b>Issue:</b>	1	<b>Revision:</b>	0

RLw	water leaving radiance reflectances
RR	Reduced resolution (1km resolution MERIS products)
RRob	Round Robin
SAFARI	Societal Applications in fisheries and Aquaculture using Remotely-sensed Imagery
SAG	Science advisory group
SDD	Secchi disk depth
SeaWiFS	Sea-viewing Wide Field-of-view Sensor (GeoEye/NASA instrument)
SoW	Statement of work
SPH	Specific Product Header
SPM	Suspended particulate material
SUM	System User Manual
SW	Software
TOA	Top of atmosphere
TOSA	top of standard atmosphere
TS	Technical specification
TSM	Total suspended matter
UCM	User consultation meeting
UML	Universal modelling language
VISAT	Visualisation and analysis tool
WFD	Water Framework Directive
WP	Work package
WPD	Work package description
XP	Extreme programming